Controlling Solvation and Mass Transport Properties of Biobased Solvents through CO2 Expansion: A Physicochemical and Molecular Modeling Study

Emanuel Granero-Fernandez, Corinne Lacaze-Dufaure, Jean-Stéphane Condoret, Vincent Gerbaud, Yaocihuatl Medina-Gonzalez

Controlling Solvation and Mass Transport Properties of Biobased Solvents through CO_2 Expansion: A Physicochemical and Molecular Modeling Study

Emanuel Granero-Fernandez,[†] Corinne Lacaze-Dufaure,[‡] Jean-Stéphane Condoret,[†] Vincent Gerbaud,[†] and Yaocihuatl Medina-Gonzalez*[,†,§]

[†]Laboratoire de Génie Chimique, Université de Toulouse, CNRS, INPT, UPS, 4 Allée Emile Monso, 31432 Toulouse Cedex 4, France

[‡]CIRIMAT, Université de Toulouse, CNRS, INPT, UPS, 4 Allée Emile Monso, BP44362, 31030 Toulouse Cedex 4, France

ABSTRACT: Gas-expanded liquids have been studied during past years; however, the physicochemical properties of some of these fluids still need to be characterized and understood. In particular, the study of properties concerning solvation and mass transport is key for industrial applications. This work presents the characterization of eight CO_2-expanded biosourced solvents: organic carbonates (dimethyl, diethyl, ethylene, and propylene carbonates), anisole, veratrole, γ-valerolactone, and 2-methyltetrahydrofuran. Two approaches have been used: spectroscopic measurements and molecular modeling. Phase equilibrium was determined for each CO_2/biosourced solvent system, and then the solvatochromic probe Nile Red was used to determine changes in dipolarity/polarizability (π^* Kamlet–Taft parameter) by CO_2 pressure. Molecular dynamics calculations were performed to determine the density and viscosity changes with CO_2 pressure. It is shown in this study that the degree of modulation of dipolarity/polarizability parameter can go from that of pure solvent (around 0.4 for linear organic carbonates) to negative values, close to that of pure CO_2 at the T and P used in this study. Concerning transport properties, such as density and viscosity, a great decrease in both these properties' values was observed after swelling of the solvent by CO_2, for instance, in linear organic carbonates where density can decrease to 50% the density of pure solvent; concerning viscosity a decrease of up to 90% was measured for these compounds. It was observed that the solubility of CO_2 and then modulation of properties were higher in linear organic carbonates than in the cyclic ones. This study shows once more that CO_2 has a great capacity to be used as a knob for triggering changes in the physicochemical properties of green biosourced solvents that can help to implement these solvents in industrial applications.

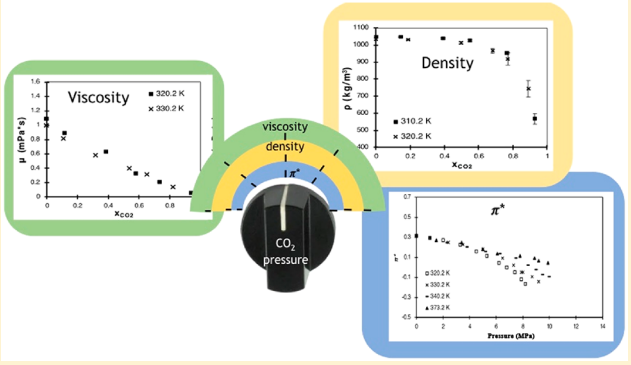

1. INTRODUCTION

The choice of a solvent is a major concern in the processes of the chemical industry. To carry out chemical reactions, the properties of the solvent to be considered are those related to the solvation of the reagents but also those related to the transport properties of the solution created, such as density, viscosity, and diffusivity, because they will strongly affect the design of the chemical reactor as well as the whole process. In addition, the potential impact on human health and the environment and the costs associated with the use and recycling of the solvent are also very important factors.

In recent decades, solvent engineering, which involves the modification or optimization of solvents, has become one of the most promising strategies for making chemical processes more sustainable. The term "green solvent", although debatable, derives from this current way of thinking and generally refers to solvents with particularly weak impact on the environment. In this group, one finds water, CO_2, solvents derived from biomass, polymers, ionic liquids, and gas-expanded liquids (GXLs).

GXLs are mixed solvents composed of a compressible gas (such as CO_2) dissolved in an organic solvent.[1] They are distinguished in particular by the adaptability and versatility of their physicochemical properties which can be strongly modified according to conditions such as pressure (P), temperature (T), and the molar fraction of CO_2 (x_{CO_2}). This allows their use in a wide range of conditions. The study of the mechanism of expansion and modulation of properties has been presented in several works in recent years.[2−5]

In the study presented here, the focus is made on a particular kind of GXLs, which are those composed by a CO_2-expanded

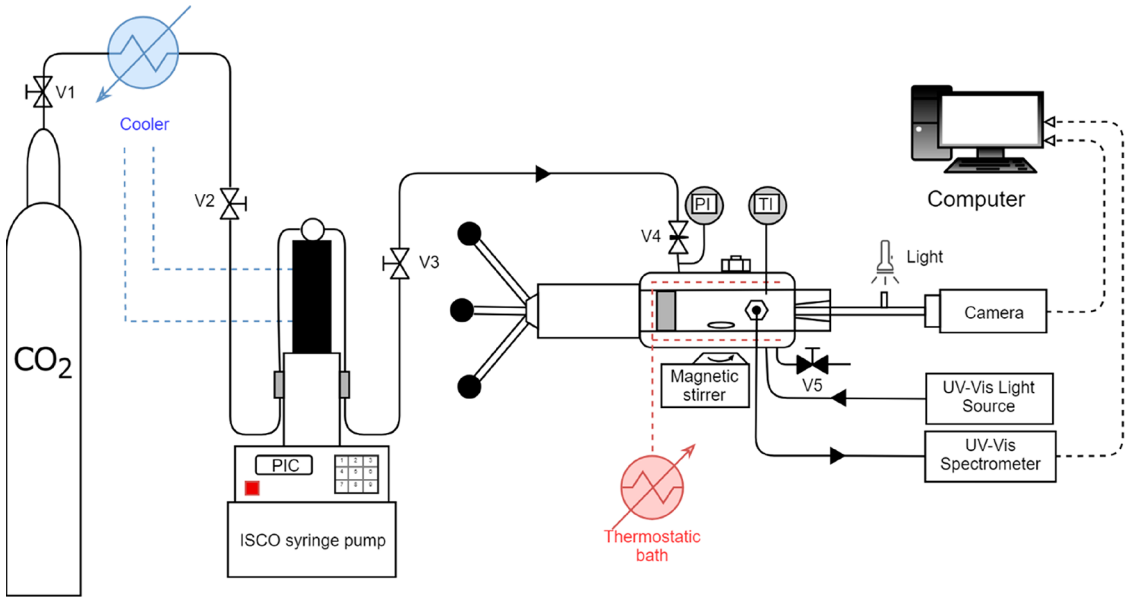

Figure 1. General scheme of the experimental device.

biosourced solvent. Some studies have already been conducted on binary systems composed of CO_2 and biosourced solvents,[6,7] but characterization and measurement of their physicochemical properties still need to be completed if some applications are envisaged at an industrial scale.

At the same time, owing to the wide range of CO_2-expanded biosourced solvents, the quantification of the properties of the solvents can be tedious and time-consuming. This is why the exploration of new methods must be considered in order to predict the properties of these systems and more systematically populate the property value diagram. In this framework, a double approach has been proposed here, where both experimental determinations and molecular dynamics simulations were carried out, in order to obtain quantitative data for these systems. From an experimental point of view, phase equilibrium and the dipolarity/polarizability Kamlet−Taft parameter through solvatochromic experiments were obtained. Density and viscosity were determined numerically by molecular dynamics calculations.

Eight CO_2-expanded biosourced solvents were studied in this work that belong to two main groups: organic carbonates (involving dimethyl, diethyl, ethylene, and propylene carbonates) and "others" (involving anisole, veratrole, γ-valerolactone, and 2-methyltetrahydrofuran). This study is an extension of the two first studies concerning the alkyl acetates family and 2-methyltetrahydrofuran (MeTHF) already performed by our group.[8,9]

2. MATERIALS AND METHODS

2.1. Experimental Determinations. The experimental measurements presented here are (1) the determination of the phase equilibrium and (2) the determination of the Kamlet−Taft π^* (dipolarity/polarizability) parameter of the expanded phase.

2.1.1. Experimental Device. The device used in this study is schematically presented in Figure 1. Before being introduced into the cell, the CO_2 was cooled to about 4 °C to ensure a liquid state; a Teledyne Isco 260D high-pressure syringe pump was used to inject the liquid CO_2 to the cell.

The experimental determinations were carried out in a high-pressure variable-volume visualization cell (9.6−31.3 cm^3, Top Industrie, France) equipped with three sapphire windows and a magnetic stirrer. The temperature of the cell was maintained at the desired value with a thermostatic bath and measured with a thermocouple (type J, accuracy of ±0.1 K) placed inside the cell. The pressure was measured by a digital manometer (Keller, LEX 1, accuracy 0.01%), equipped with a digital pressure display. For dipolarity/polarizability parameter determinations, the high-pressure cell was coupled to an EPP2000 UV−vis spectrometer from StellarNet Inc. equipped with optical fibers and an Ocean Optics DH-2000 light source.

2.1.2. Phase Equilibrium Determinations. In the study of the phenomenon of expansion of liquids, the information on the composition of the phases at equilibrium is the essential starting point for numerical determinations. This information can be (i) obtained from the literature, (ii) predicted with a certain degree of precision with an equation of state, and (iii) obtained from physical experiments. For some of the studied expanded binary systems, the equilibrium compositions for the expanded phase were obtained with the synthetic method[10] described below.

The method used for the determination of phase equilibrium was similar to that used by Crampon et al.,[11] who measured the solubility of fatty acid esters in CO_2. A known volume of the studied solvent, usually 10.0 mL, was introduced into the cell at the desired temperature. The air still inside was evacuated by reducing the volume of the cell to the point where there were no more air bubbles. The CO_2 was then injected with the Isco pump, and the volume was gradually increased by moving back the piston of the cell to allow the entry of the gas. Once the desired amount of CO_2 was injected, a first equilibrium was achieved in two phases with vigorous stirring. Then, the pressure was adjusted with the piston by decreasing the volume of the cell to the point where there was only one phase, at a higher pressure. Once the system was equilibrated, the volume was increased slightly to reveal a second phase. The system was then compressed and decompressed successively to define the narrowest pressure range to evaluate the phase transition pressure. This procedure was repeated for each point in the $P-x$ diagram.

The temperature was measured with an accuracy of ±0.1 K, and the pressure was measured with an accuracy of ±0.02 MPa for pressures up to 10 MPa and 0.05 MPa for higher pressures. The error in molar fraction mainly concerns CO_2, and was estimated to be less than 0.003.[10]

2.1.3. Dipolarity/Polarizability Kamlet–Taft Parameter Determinations. The dipolarity/polarizability has been studied through the determination of Kamlet–Taft parameters[12−15] of the liquid (expanded) phase at vapor–liquid equilibrium (VLE). These parameters are based on the solvatochromic effect of certain molecules, called solvatochromic probes, which show a change at the electronic level as a function of the dipolarity of the medium, inducing a modification of the absorption spectrum. For the determination of the dipolarity/polarizability parameter (π^*), the change in the wavelength of maximal absorbance by the solvatochromic probe in the medium to be studied at the desired P, T, and composition may be a hypsochromic displacement (shorter wavelength = weaker dipolarity) or a bathochromic shift (longer wavelength = stronger dipolarity). When one increases the concentration of CO_2 at constant temperature, usually the dipolarity/polarizability decreases and so does the wavelength.

In this work, the molecule used as a probe is the Nile Red dye (9-diethylamino-5-benzo[a]phenoxazinone) (Figure 2).

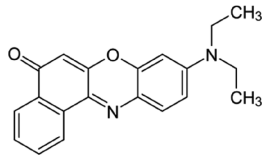

Figure 2. Red Nile solvatochromic probe representation.

Determination of the π^* parameter of the expanded phase at VLE by measurement of the solvatochromism was carried out in the variable-pressure high-pressure cell already described. The spectrometer was connected to two of the windows of the cell through optical fibers.

The measurement started with the addition of a known volume, usually 10.0 mL, of the solvent in the cell at the desired temperature, with constant stirring. The spectrometer was then used to generate the control blank, with and without the light source.

Once this blank was generated, the solvatochromic probe was added to the cell and dissolved in the solvent. A concentration of Nile Red dye was used so that its absorption spectrum was neither too weak for a correct reading nor too high to saturate the detector. This concentration was still very low (about 0.001 M), and therefore its effect on the expansion of the liquid was considered as negligible.

Then, the free space inside was reduced by the movement of the piston and the air was flushed with CO_2 before the cell was closed. The pressure was then increased with the injection of CO_2 with the Isco pump and the volume was increased gradually to allow the existence of two phases. For each point, equilibrium was considered as reached when the pressure value was stable during more than 1 h. The absorption spectra were then recorded.

For these determinations, the molar fractions in each phase were obtained from the liquid–vapor equilibrium diagrams.

2.1.4. Materials. The different chemical compounds used in the experiments are listed in Table 1 with their suppliers and purities. All of these compounds were used as delivered.

2.2. Numerical Determinations. Molecular dynamics (MD) simulations were carried out to calculate different properties of the expanded phases of these binary systems. The determinations of density and viscosity for these CO_2-expanded systems were performed in the *NPT* and *NVE* ensembles, respectively. These calculations have been performed for the liquid phase at experimental VLE.

After numerous tests of all the force-field potentials available in the MAPS suite[16] and in the LAMMPS software, the Amber Cornell Extended (ACEFF) potential, a property of Scienomics, was chosen as the best option. This potential is well-suited to describe nonreactive systems like those studied here by combining inter- and intramolecular terms (Table 2).

Table 2. Amber Cornell Extended Potential (Scienomics)

bond	$E_{\text{bond}} = \sum K_b(b - b_0)^2$
angle	$E_{\text{angle}} = \sum K_\theta(\theta - \theta_o)^2$
improper	$E_{\text{improper}} = \sum K_\varphi(\varphi - \varphi_0)$
dihedral	$E_{\text{dihedral}} = \sum K_\chi[1 + \cos(n\chi - \delta)]$
van der Waals: Lennard-Jones (12–6)	$E_{\text{LJ}} = \sum 4\varepsilon_{ij}\left[\left(\frac{R_{\min,ij}}{r_{ij}}\right)^{12} - \left(\frac{R_{\min,ij}}{r_{ij}}\right)^{6}\right]$
electrostatic: Coulomb	$E_{\text{Coulomb}} = \sum \frac{q_i q_j}{\varepsilon r_{ij}}$

Concerning the *NVE* simulations, the Nose–Hoover thermostat was used and a temperature damping parameter of 10 fs (T_{damp}) was assigned. *NPT* simulations were carried out by using the Nose–Hoover thermostat with isobaric conditions which

Table 1. Materials, Suppliers, and Purities

compound	chemical formula	supplier	purity
anisole	$C_6H_5OCH_3$	Acros Organics	99%
veratrole	$C_6H_4(OCH_3)_2$	Acros Organics	>99%
γ-valerolactone	$C_5H_8O_2$	Acros Organics	98%
dimethyl carbonate	$(CH_3O)_2CO$	Acros Organics	99%
diethyl carbonate	$(OCH_2CH_3)_2OC$	Acros Organics	99%
ethylene carbonate	$C_3H_4O_3$	Acros Organics	>99%
propylene carbonate	$C_4H_6O_3$	Acros Organics	99.5%
2-methyltetrahydrofuran	$CH_3C_4H_7O$	Sigma-Aldrich	>99%
Nile Red	$C_{20}H_{18}N_2O_2$	Sigma-Aldrich	technical grade
carbon dioxide	CO_2	Air Liquide	>99%

were fulfilled using the method of Martyna and co-workers[17a] with a T_{damp} of 10 fs and a stress damping parameter (P_{damp}) of 350 fs used, respectively. Both T_{damp} and P_{damp} are in the recommended range of damp values for nonmetal systems. The Verlet algorithm was used for time integration.

In Table 2, b is the bond length, θ is the valence angle, χ is the dihedral angle, ϕ is the out-of-plane torsion angle, and r_{ij} is the distance between atoms i and j. The bond and the valence angle contributions are calculated using a harmonic functional form, which assumes values oscillating relatively close to equilibrium. The parameters associated with this assumption are the bond force constant K_b, the equilibrium bond length b_0, the valence angle force constant K_θ, and the equilibrium valence angle θ_0. The potential energy due to rotation about bonds or torsions is calculated through the dihedral angle, with K_χ the dihedral force constant; the multiplicity n is the periodicity dictating the number of cycles per 360° and δ is the phase angle. The potential energy associated with out-of-plane torsions or improper angles is calculated harmonically as well; its parameters include the improper angle force constant $K_{improper}$ and the equilibrium improper angle term ϕ_0. The nonbonded terms include the van der Waals (VdW) and the electrostatic interactions energy; the VdW contribution is calculated using a Lennard-Jones 6−12 function, where the repulsive term is a hard well potential of $1/r^{12}$ and the attractive term is $1/r^6$. The interaction parameters ε_{ij} and $R_{min,ij}$ describe, respectively, the Lennard-Jones well depth and the minimum interaction distance between atoms i and j. The electrostatic contribution to the potential energy is calculated by using Coulomb's law, where q_i and q_j are the partial atomic charges of the atoms and ε is the dielectric constant of the solvent, which in the case of explicit solvent representation is set to 1.

2.2.1. Calculation of Coulombic Charges. The geometries of the molecules of the eight solvents tested were optimized in the gas phase in the framework of density functional theory (DFT) at the B3LYP/6-31+G** level of theory (Gaussian 09[17b]).

Atomic charges were fitted to the electrostatic potential (ESP) in agreement with the Merz−Singh−Kollman scheme.[18,19] For the CO_2 molecule the Harris−Yung model was used.[20]

2.2.2. Calculation of the Statistical Error. This error was calculated by calculating the standard deviation of the block data After the stabilization phase, when the actual data production phase was started, the total number of calculation steps was divided into blocks of 10 000 steps. The average of these 10 000 steps was recorded (x). At the end of the simulation, the standard deviation (σ) (eq 1) was calculated on the recorded values (x = average for a block of 10 000 steps).

$$\sigma = \sqrt{\frac{1}{N}\sum_{i=1}^{N}(x_i - u)^2} \tag{1}$$

For example, for the more typical case of 1 200 000 total computation steps, at the end, a group of N = 120 x values is obtained from which is calculated the standard deviation together with the mean or true value u (average of all x values).

The simulation conditions are summarized in Table 3. In general, a simulation exhibits two stages: start/stabilization and production of results. When a simulation is started, the atomic positions and the orientation of the molecules are randomly given and their velocities are assigned in order to correspond to the temperature of the system (Maxwell−Boltzmann distribution). However, this initial configuration is not at equilibrium and is therefore not stable. The first step is thus a minimization of energy. Once the equilibrium energy is reached, the second step, the production of results, starts. It is a period of time during which the simulation is carried out to adequately sample the states of the system and which depends on the property to be determined.[21]

Table 3. MD Simulations Conditions for Density Determination

ensemble	*NVT* for equilibrium; *NPT* for results production
time step	1 fs
total number of molecules	1000
total steps	1 200 000
cutoff distance	8 Å
switching distance	12 Å
initial velocities	randomly assigned
border conditions	periodical
long-range iteractions	PPPM[a]

[a]Particle−particle particle-mesh solver.

The isobaric−isothermal ensemble (*NPT*) allows us to determine density through volume fluctuations. All the studied systems were at conditions of T, P, and CO_2 concentration corresponding to the liquid phase at the liquid−vapor equilibrium obtained experimentally in this work and compared to existing literature data, because the objective was to be able to modulate experimentally the properties of the expanded phase through the CO_2 pressure.

2.2.3. Determination of Viscosity by Molecular Dynamics. The fluctuation−dissipation theorem explains how the transport coefficients associated with irreversible processes can be described using reversible microscopic fluctuations.[22] Green−Kubo's relations[23,24] give the exact mathematical expression of the transport coefficients in terms of integrals of the temporal correlation functions.

In the standard Green−Kubo method, the dynamic viscosity (shear) of a fluid expresses its resistance to shear flow where adjacent layers move parallel to each other at different speeds. It can be calculated by integrating the function of autocorrelation of the stress tensor over time as in eq 2.

$$\eta = \frac{V}{k_B T}\lim_{\tau\to\infty}\int_0^\tau \langle P_{xy}(t)\, P_{xy}(0)\rangle \, dt \tag{2}$$

where $\langle P_{xy}(t)\ P_{xy}(0)\rangle$ is the correlation function of the xy component of the stress tensor, V is the volume of the simulation box, k_B is Boltzmann's constant, T is the absolute temperature, and t is time. This method was shown to be efficient for calculating the viscosity of pure components and mixtures.[25−29]

3. RESULTS AND DISCUSSION

3.1. Phase Equilibria of CO_2-Expanded Systems. The temperatures at which the phase equilibria were determined were first selected in accordance with available literature data to check the validity of the method. Then new data were obtained for other temperatures, within the technical limits of our device (from ambient to 393.15 K).

All the determinations are presented below in the form of P−x_{CO_2} diagrams, grouped according to the two selected groups of solvents, along with the available literature data. Due to the 0.1 K accuracy of the temperature sensor, all temperatures were rounded to the first decimal.

Solubility values of CO_2 in the solvents are shown as isotherm curves in Figures 3−12. In all cases these isotherms show that, as

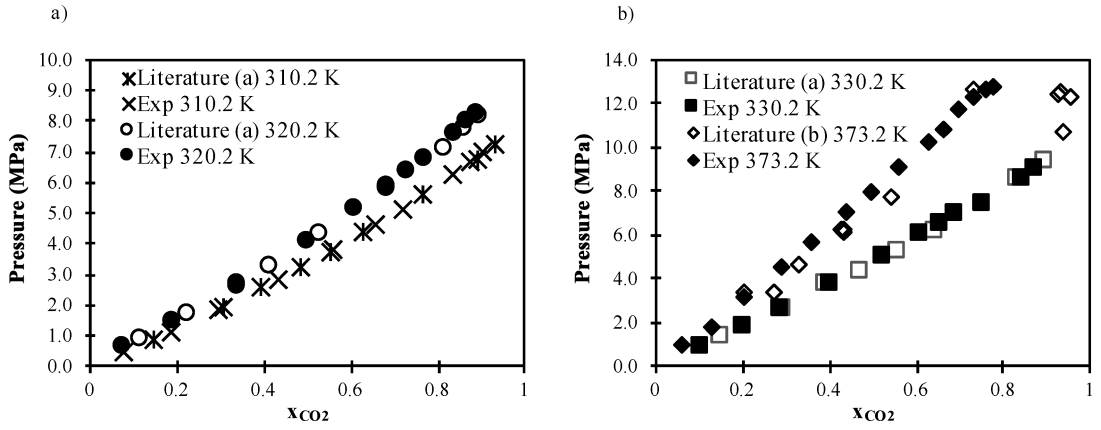

Figure 3. $P-x_{CO_2}$ diagram for CO_2 + dimethyl carbonate system: (a) 310.2 and 320.2 K; (b) 330.2 and 373.2 K. Data taken from refs (a) 30 and (b) 31.

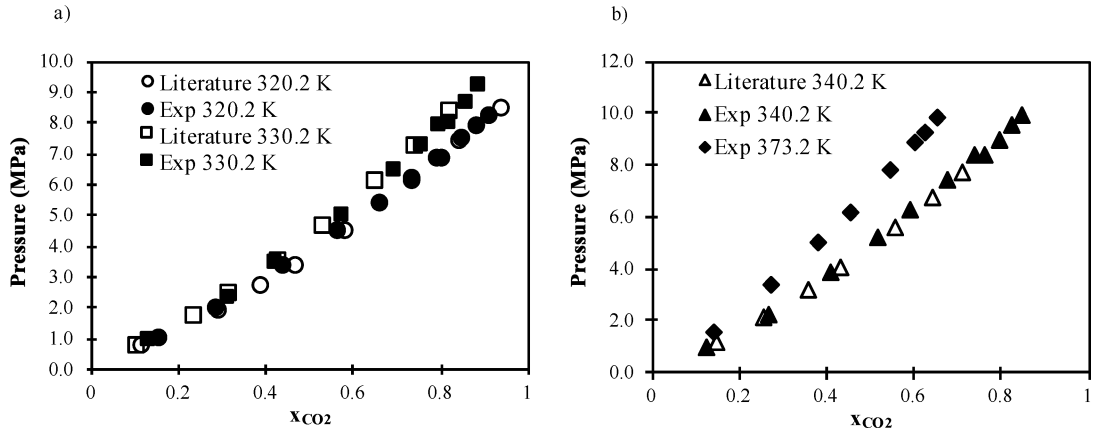

Figure 4. $P-x_{CO_2}$ diagram for CO_2 + diethyl carbonate system: (a) 320.2 and 330.2 K; (b) 340.2 and 373.2 K. Data taken from ref 30.

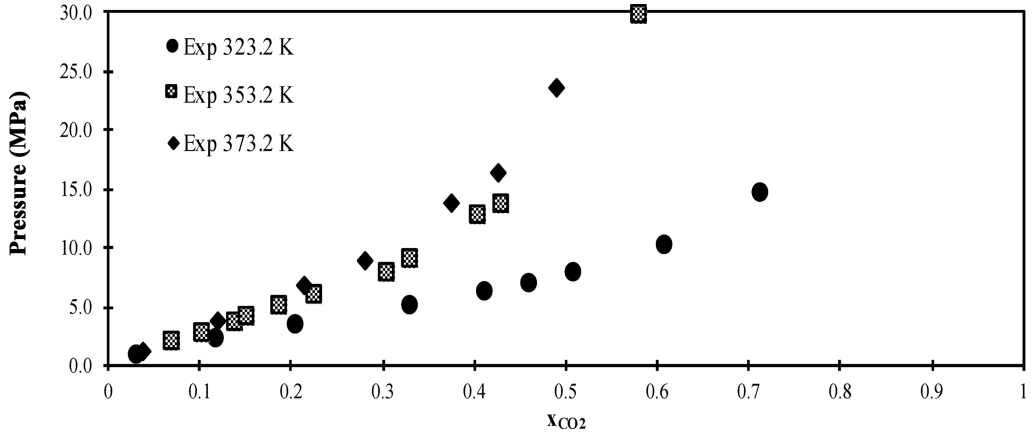

Figure 5. $P-x_{CO_2}$ diagram for CO_2 + ethylene carbonate system at 323.2, 353.2, and 373.2 K.

expected, the molar fraction of the dissolved gas increases with the pressure and decreases with temperature. However, the nature of each solvent constrains its behavior when in mixture with a gas and, particularly, with CO_2.

Regarding the validation of the measurements, available literature data were plotted and, in almost all cases, were in good agreement with our experimental determinations.

3.1.1. Phase Equilibria of CO_2-Expanded Organic Carbonates. The phase equilibrium diagrams for the organic carbonates are presented in Figures 3–6.

For cyclic carbonates (ethylene and propylene carbonates) it was observed that the CO_2 solubility was significantly lower than for linear carbonates (dimethyl and diethyl carbonates).

The isotherm for the CO_2 + propylene carbonate system at 373.2 K (Figure 6b) shows the most noticeable difference between literature data and our determinations. This can be partly explained by the experimental difficulty for systems with low CO_2 solubility and from the visual method used for the phase equilibrium determination in both cases.

All the solvents studied here are class II biosourced organic solvents of the Jessop et al.[1] classification. This group comprises

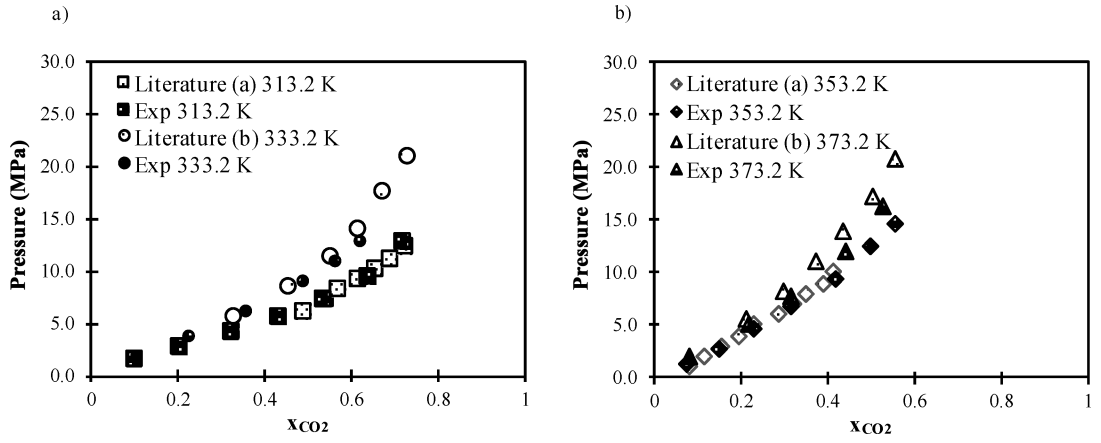

Figure 6. $P-x_{CO_2}$ diagram for CO_2 + propylene carbonate system: (a) 313.2 and 333.2 K; (b) 353.2 and 373.2 K. Data taken from refs (a) 32 and (b) 33.

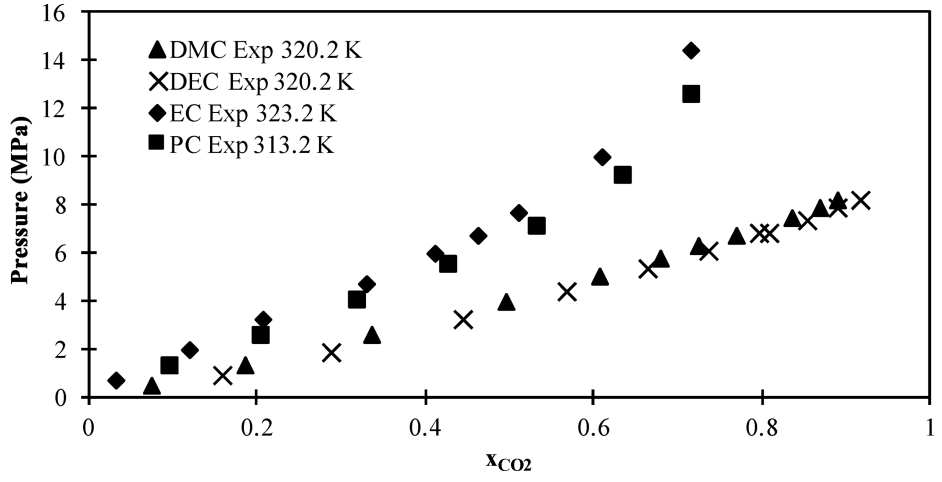

Figure 7. $P-x_{CO_2}$ diagrams for CO_2 + organic carbonates systems at temperatures nearest to 320.2 K. DMC, dimethyl carbonate; DEC, diethyl carbonate; EC, ethylene carbonate; PC, propylene carbonate.

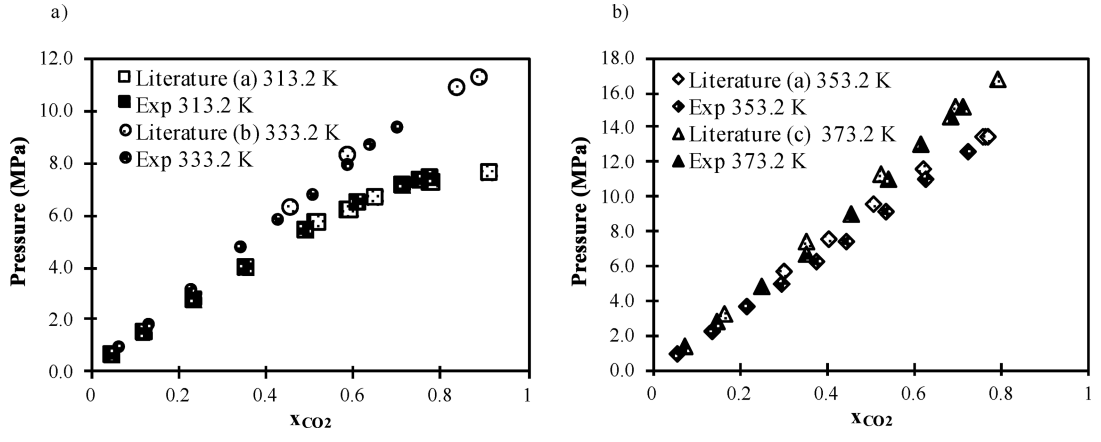

Figure 8. $P-x_{CO_2}$ diagram for CO_2 + anisole system: (a) 313.2 and 333.2 K; (b) 353.2 and 373.2 K. Data taken from refs (a) 34, (b) 35, and (c) 36.

liquids capable of solubilizing moderate to high amounts of CO_2 and possibly increasing their volumes up to several times. However, their behaviors with respect to CO_2 can be very different in some cases. For example, the analysis of the curves for organic carbonates, at a temperature close to 320.2 K (Figure 7), shows a significant difference between linear carbonates (dimethyl carbonate and diethyl carbonate) and cyclic carbonates (ethylene carbonate and propylene carbonate).

3.1.2. Other CO_2-Expanded Biosourced Solvents Phase Equilibrium. The phase equilibrium diagrams for anisole, veratrole, γ-valerolactone and MeTHF when expanded by CO_2 are presented in Figures 8−11.

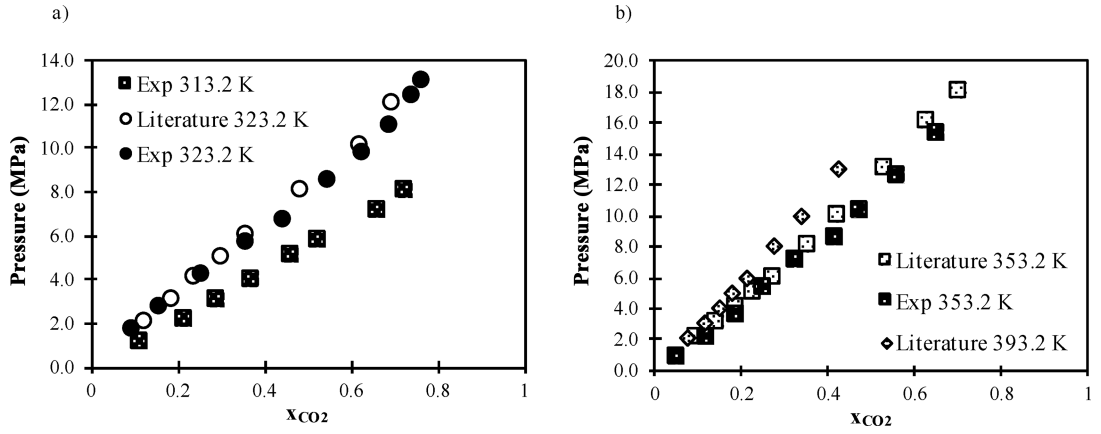

Figure 9. $P-x_{CO_2}$ diagram for CO_2 + veratrole system: (a) 313.2 and 323.2 K; (b) 353.2 and 393.2 K. Data taken from ref 37.

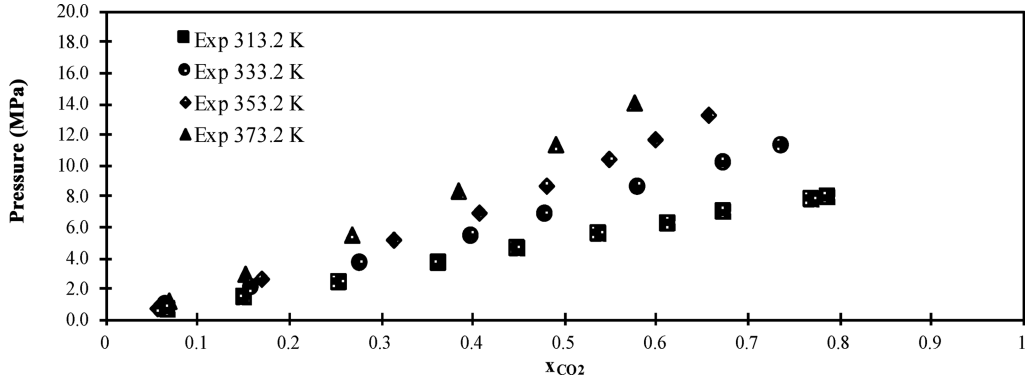

Figure 10. $P-x_{CO_2}$ diagram for CO_2 + γ-valerolactone system at 313.2, 333.2, 353.2, and 373.2 K.

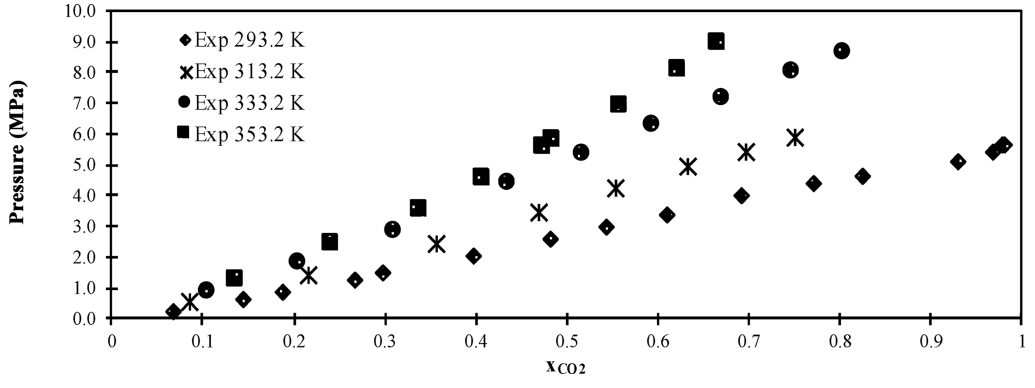

Figure 11. $P-x_{CO_2}$ diagram for CO_2 + 2-methyltetrahydrofuran system at 293.2, 313.2, 333.2, and 353.2 K.

MeTHF exhibits a very high solubility for CO_2, and therefore it was possible to reach a high concentration of dissolved CO_2 for relatively low or moderate pressures.

The evaluation of the solubility of CO_2 in the organic solvents studied here indicates that, to reach a given concentration of the gas in the expanded liquid phase, it will logically require a higher or lower pressure depending on the affinity and the capacity of the solvent to accept the CO_2 molecules.

As a reminder, the classification used for GXLs is based on the solubility of CO_2 and the volume expansion associated with it.[1] For the case of MeTHF (Figure 11), the needed pressure to reach a mole fraction of 0.5 at a temperature close to ambient (298.2 K) is relatively low (2.5−3.0 MPa). For anisole (Figure 8), veratrole (Figure 9), and γ-valerolactone (Figure 10) at 313.2 K, the needed pressure for this same molar fraction is very similar for these three compounds (5.0−5.5 MPa at 313.2 K). Ethylene and propylene carbonates, members of the cyclic organic family (Figures 5 and 6), have lower solubilities and therefore the needed pressure is significantly higher, which places these two solvents in the limits of class II (high solubility and volume expansion) and perhaps close to class III (moderate solubility and volume expansion), a class whose ionic liquids are the most representative components.[38] For the CO_2 + ethylene carbonate system (Figure 12a), the presence of a zone of immiscibility can be suspected, since the equilibrium pressure seems to increase very rapidly from x_{CO_2} = 0.6.

For all the $P-x_{CO_2}$ diagrams studied here, a quasi-linear relationship is observed for the low pressures and CO_2 concentrations (below x_{CO_2} = 0.2). For example, for the CO_2

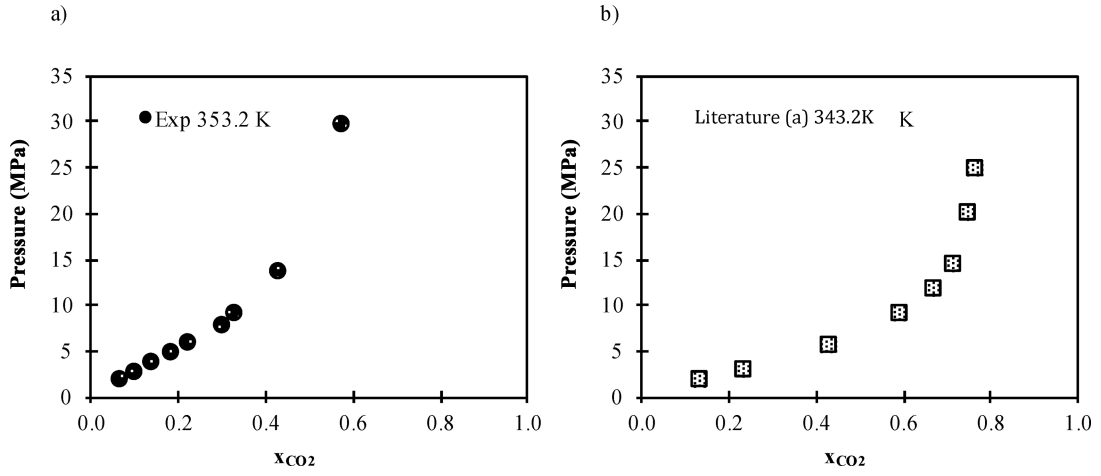

Figure 12. $P-x_{CO_2}$ diagrams for CO_2 + ethylene carbonate system at 353.2 K and CO_2 + [HMIm][Tf_2N] system at 343.2 K. Data taken from ref 39.

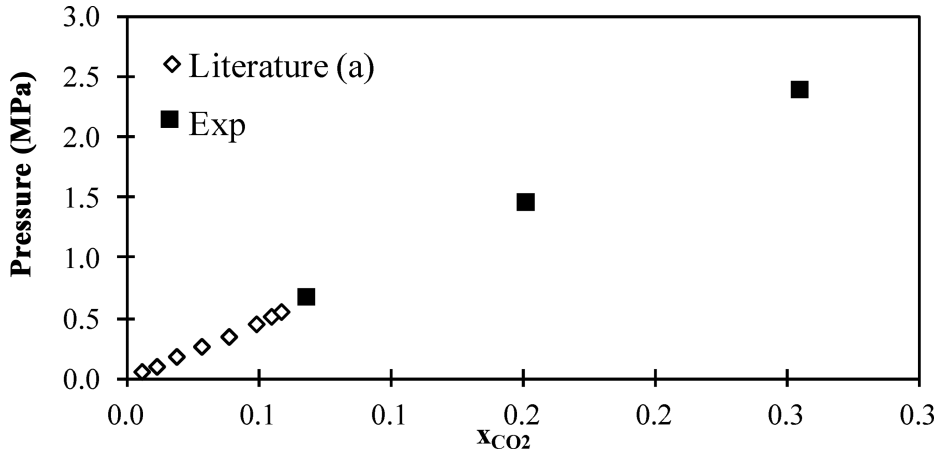

Figure 13. $P-x_{CO_2}$ diagram for CO_2 + γ-valerolactone system at low concentrations at 313.2 K. Data taken from ref 40.

Table 4. Henry's Constants (K_H) and Validity Intervals for Different Solvents at Different Temperatures

solvent	T (K)	K_H (MPa)	validity interval (max x_{CO_2})	T (K)	K_H (MPa)	validity interval (max x_{CO_2})
dimethyl carbonate	310.2	5.76	0.4	330.2	8.31	0.4
	320.2	7.48	0.4	373.2	16.66	0.4
diethyl carbonate	320.2	6.04	0.15	340.2	7.6	0.2
	330.2	7.2	0.2	373.2	10.47	0.15
ethylene carbonate	323.2	22.71	0.4	373.2	32.17	0.2
	353.2	24.83	0.2			
propylene carbonate	313.2	12.38	0.15	353.2	17.75	0.2
	333.2	14.3	0.15	373.2	23.01	0.2
anisole	313.2	11.49	0.35	353.2	16.3	0.3
	333.2	12.83	0.2	373.2	18.57	0.3
veratrole	313.2	9.55	0.1	353.2	20.83	0.2
	323.2	15.69	0.1	393.2	27.51	0.2
γ-valerolactone	313.2	7.79	0.35	353.2	14.06	0.2
	333.2	12.92	0.35	373.2	17.84	0.2
2-methyltetrahydrofuran	293.2	4.21	0.4	333.2	8.46	0.3
	313.2	6.5	0.4	353.2	9.66	0.25

+ γ-valerolactone system, in Figure 13, the low concentration behavior, in agreement with Deng et al.,[40] would make it possible to use a "Henry's law"-like equation where at constant temperature the quantity of gas dissolved in a liquid is proportional to the partial pressure exerted by the gas on the liquid. This proportionality exists mainly at low pressures. Deng et al.[40] have calculated Henry's constants for CO_2 for several biosourced solvents.

At low temperature, when the solvent partial pressure is negligible, it is assumed that the total pressure (P) is equal to the partial pressure of CO_2 (P_{CO_2}) due to the low volatility of the GVL. A rapid analysis of the solubility data makes it possible to

Temperature (K)	λ_{max} (nm)
310.2	516
320.2	515
330.2	514
373.2	509

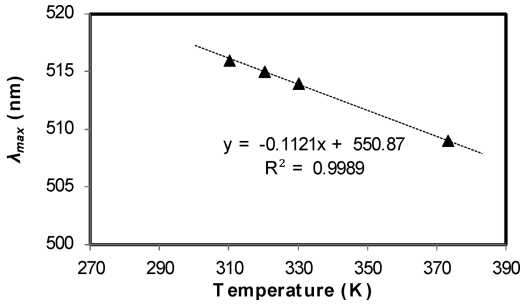

Figure 14. Variation of λ_{max} with temperature for Nile Red dye in dimethyl carbonate.

estimate values of Henry's constant (K_H), which in turn allows us to estimate the quantity of gas dissolved in the liquid using eq 3.

$$P_{CO_2} = x_{CO_2} K_H \tag{3}$$

The K_H values are presented in Table 4 for each solvent, with the determination temperature (T) and a validity interval, corresponding to the interval where the linear fitting of the curve yielded a value of the regression coefficient greater than 0.999.

Finally, if solubilities of CO_2 in linear carbonates (dimethyl and diethyl carbonates) and in cyclic carbonates (ethylene and propylene carbonates) are compared, it is observed that cyclic carbonates present lower solubilities of CO_2 than linear carbonates.

3.2. Dipolarity/Polarizability of the CO_2-Expanded Systems. The relationship between the π^* of the medium and the wavelength absorbed by the Nile Red dye was studied by Mistry et al.,[41] who evidenced the difference between protic solvents (or hydrogen-bonding donors, HBD) and aprotic solvents (either non-hydrogen bonding or hydrogen bond acceptor, NHB). Thus, all alcohols are set apart in the HBD group while ethers, esters, carbonates, etc. are referenced as NHBs. These authors compared the π^* parameters of several solvents and thus obtained a single equation allowing computation of the values of π^* (eq 4) from the maximal absorption wavelength (λ_{max}), where λ_{max} must be expressed in nanometers.

$$\pi^* = \frac{(\lambda_{max}{}^{-1} \cdot 10000) - 19993}{-1724} \tag{4}$$

3.2.1. Thermochromism. The probe used in solvatochromic measurements, Nile Red dye, exhibits a particular behavior in solution with temperature changes, in parallel with changes in the surrounding media dipolarity/polarizability. This phenomenon, called "thermochromism",[42,43] must be taken into account when calculating π^* values.

All the determinations presented in this work were made at constant temperature, but the experimental determinations had to be adjusted according to this thermochromism phenomenon. In Figure 14 we can observe the variation of the λ_{max} of Nile Red in dimethyl carbonate with temperature.

It is important to note also that the accuracy of the spectrometer is 1 nm, which will have consequences on the accuracy of the π^* "corrected" values.

Thermochromism was evaluated in all solvents at the different temperatures studied here, and its effect evaluated relatively linear in all cases. This linear response of Nile Red dye has been reported in the literature for some solvents such as acetone.[42]

The thermochromic relationships are displayed for all solvents in Table 5 as a linear function $f(x) = ax + b$.

Table 5. Thermochromism Relationships for All the Solvents Concerned Here

solvent	abbrev	a	b	R^2
dimethyl carbonate	DMC	−0.1121	550.87	0.9989
diethyl carbonate	DEC	−0.1142	548.70	0.9978
ethylene carbonate	EC	−0.1142	581.43	0.9868
propylene carbonate	PC	−0.1000	569.32	1.0000
anisole	Ani	−0.2000	593.14	0.9877
veratrole	Vera	−0.1395	579.13	0.9989
γ-valerolactone	GVL	−0.1000	569.32	1.0000
2-methyltetrahydrofuran	MeTHF	−0.1950	580.27	0.9909

The value of the slope a lies between those of carbonates (about −0.1 nm/K) and MeTHF (−0.195 nm/K). It is important to note that despite the general behavior of the Nile Red dye, whose λ_{max} decreases with temperature in all the solvents studied here, there is no constant value for this variation and a general equation cannot be established because it depends on the nature of the solvent. Among the causes that explain the temperature-dependent changes in the UV−vis absorption spectrum, there are the effect of temperature in the refractive index of the solvent, the effect of temperature on the Boltzmann distribution between the vibrational and rotational energy levels of a solute molecule, and the temperature-dependent interactions between molecules, such as hydrogen bonding interactions.[44] As formation of hydrogen bonds increases with decreasing temperature, Nile Red dye will then be differentially affected by temperature, depending on the nature of the solvent and its ability to form hydrogen bonds or not.[44]

Once the values of λ_{max} are corrected with the thermochromic relationships obtained for the different pure solvents (Table 5), values of the π^* parameter can be calculated with the help of eq 4.

The reference temperature (T_{ref}) used to calculate the value of π^* for each pure solvent was 298.2 K, with the exceptions of 2-methyltetrahydrofuran, for which it was 293.2 K, and ethylene carbonate, where π^* was calculated at 323.2 K due to its higher melting point.

3.2.2. Determination of the π^* Parameter. The multiparameter scale of Kamlet−Taft combines the dipolarity and the polarizability of the surrounding medium of a solute in the single π^* parameter. In this view, π^* was evaluated for pure and CO_2-expanded solvents.

For pure solvents, Table 6 presents the values of π^* calculated with eq 4 at the reference temperature, with the values available

Table 6. Calculated vs Literature π^* Parameters for Pure Solvents[a]

solvent	calcd π^*	T_{ref} (K)	lit. π^*	error	ref
dimethyl carbonate	0.38	298.2	0.38	0.0	45
diethyl carbonate	0.31	298.2	0.45	−0.14	45
ethylene carbonate	0.91	323.2	–	–	–
propylene carbonate	0.85	298.2	0.83	0.02	45
anisole	0.73	298.2	0.73	0.0	45
veratrole	0.81	298.2	–	–	–
γ-valerolactone	0.85	298.2	0.83	0.02	46
2-methyltetrahydrofuran	0.50	293.2	0.53	−0.03	46
$scCO_2$ (9 MPa, 60 °C)	–	–	−0.47	–	46
$scCO_2$ (100 MPa, 60 °C)	–	–	−0.03	–	46

[a]Values for CO_2 have been included for comparison.

in the literature. The accuracy of the spectrometer is 1 nm, which leads approximately to an accuracy of 0.025 for π^*.

In Figures 15−24 it can be observed how π^* decreases with the pressure giving rise to a wide range of accessible polarities for the expanded system, both positive and negative, thus highlighting the extent of modulation of this parameter for these systems.

3.2.3. π^* of CO_2-Expanded Organic Carbonates. The results of the determination of the π^* parameter in organic carbonates are shown in Figures 15−18 at different temperatures.

For cyclic carbonates, the change in the π^* parameter occurred at much higher pressures, since the solubility of CO_2 is considerably lower as mentioned in section 3.1. At the same time, the π^* of the pure solvent is also higher.

In the case of organic carbonates, the first difference that is observed is a strong variation of the dipolarity/polarizability for the linear carbonates (dimethyl carbonate and diethyl carbonate), whereas this is less marked in the case of cyclic carbonates (ethylene carbonate and propylene carbonate). For these latter, it is necessary to implement higher pressures, probably because of the lower solubility of CO_2 in these pure solvents. Since the π^* parameter of the pure carbonates is very different, it is preferable to use the ratio between π^* and $\pi^*_{P=0}$ at the relative pressure of P = 0 MPa, at the nearest available temperature of 320.2 K (Figure 19).

When comparing the extent of modulation of π^* for the organic carbonates tested, the trend dimethyl carbonate ≈ diethyl carbonate > propylene carbonate > ethylene carbonate can be observed and follows the same trend observed when comparing CO_2 solubilities (Figure 7). Note that, in the case of cyclic carbonates, CO_2 reaches negative values for π^*, near those of pure CO_2, while for CO_2-expanded cyclic carbonates, values of π^* remain positive.

By comparing the π^* data for solvents with or without expansion, it is seen that the expansion of the solvents by the gas makes it possible to obtain significant changes in the properties of the solvent that can go as low as π^* values less than zero. The data reported here seem to contradict those reported by Wyatt et al.[47] where the solvatochromic parameters of the GXLs appeared fairly constant and similar to those of the pure liquid, even at high concentrations of CO_2. However, their study was limited to two expanded solvents, methanol and acetone.

3.2.4. π^* Parameters of Anisole, Veratrole, γ-Valerolactone, and MeTHF Expanded by CO_2. Finally, the results for the determination of the π^* parameter values for solvents other than organic carbonates are shown in Figures 20−24, with a scale of 0−1 for π^*.

It is now well demonstrated that the dipolarity modulation produced by the presence of CO_2 strongly depends on its solubility in the pure solvent. However, this is not the only factor, because the nature of the solvent also plays a role.

The nonlinearity of the variation of the dipolarity as a function of the mole fraction of CO_2 in most solvents studied here, mainly at low temperatures, can also be explained by the increased presence of the solvent molecules in the cybotactic region (i.e., molecules surrounding the solute) of Nile Red dye, with respect to the CO_2 presence, yielded a modified local composition. In other words, Nile Red will be surrounded according to its affinity for the solvent and CO_2 in a different proportion than the bulk composition. This effect is known as preferential solvation[48−50] and has been suggested to be responsible for the nonlinearity of excitation energies (responsible for solvatochromism) in other binary mixtures[51,52] and other CO_2-expanded solvents, as evaluated from physical experiments and simulations.[53,54]

3.3. Densities of CO_2-Expanded Systems. The solvents studied here have significant differences in their ability to solubilize CO_2, even if they all fall into the "class II" category of

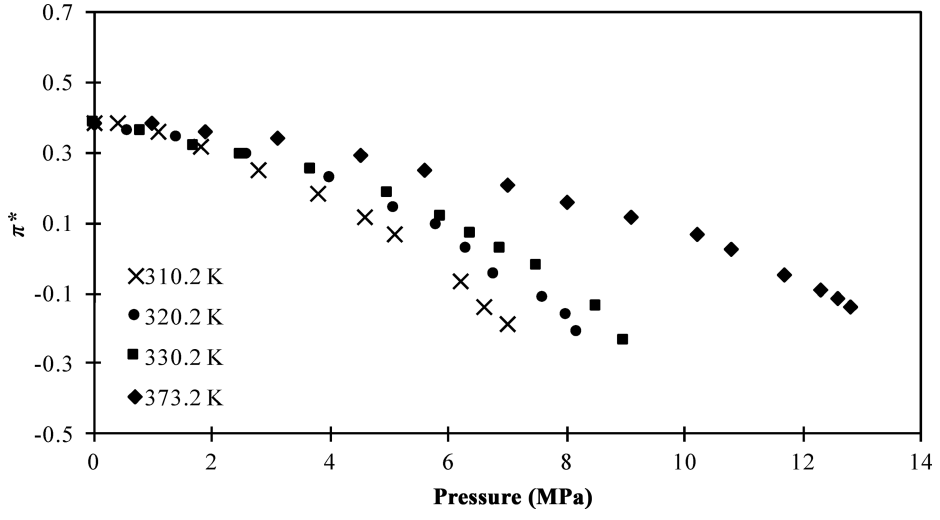

Figure 15. Variation of π^* parameter as a function of CO_2 pressure for CO_2 + dimethyl carbonate system at different temperatures.

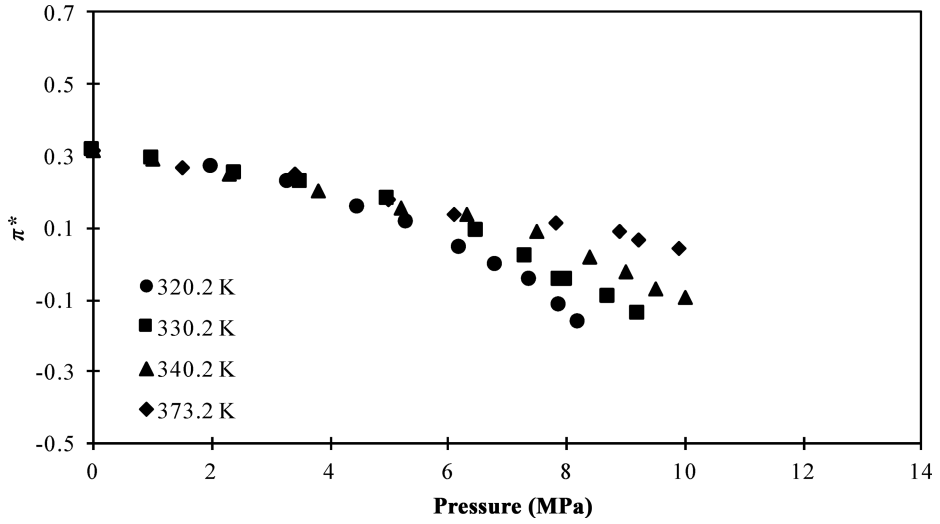

Figure 16. Variation of π^* parameter as a function of CO_2 pressure for CO_2 + diethyl carbonate system at different temperatures.

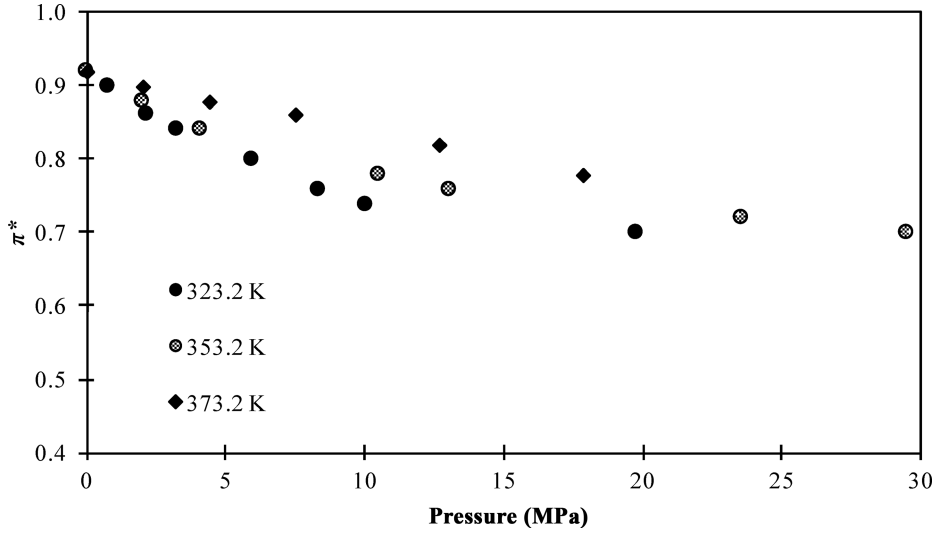

Figure 17. Variation of π^* parameter as a function of CO_2 pressure for CO_2 + ethylene carbonate system at different temperatures.

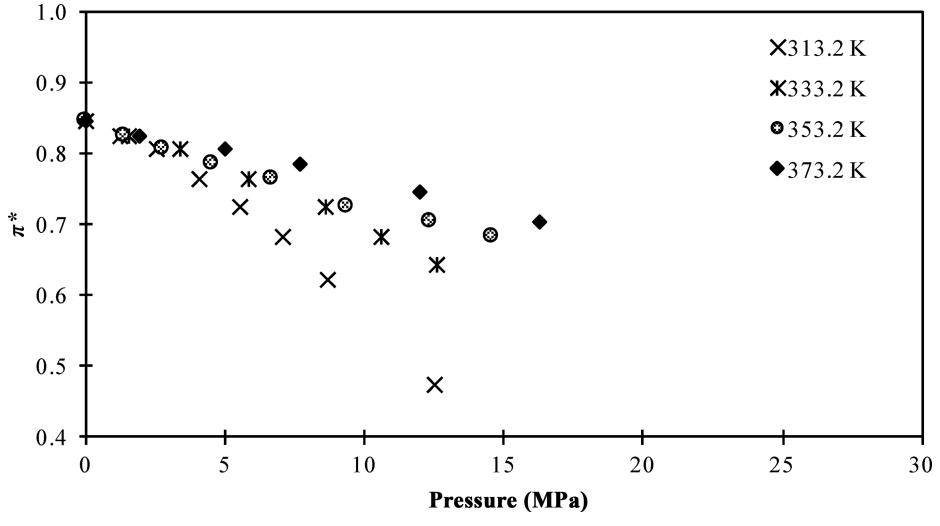

Figure 18. Variation of π^* parameter as a function of CO_2 pressure for CO_2 + propylene carbonate system at different temperatures.

the Jessop et al.[1] classification. Besides, one notices that the increase in volume is not proportional to the amount of material in the system, which means that the density of the expanded systems is not proportional to the gas concentration.

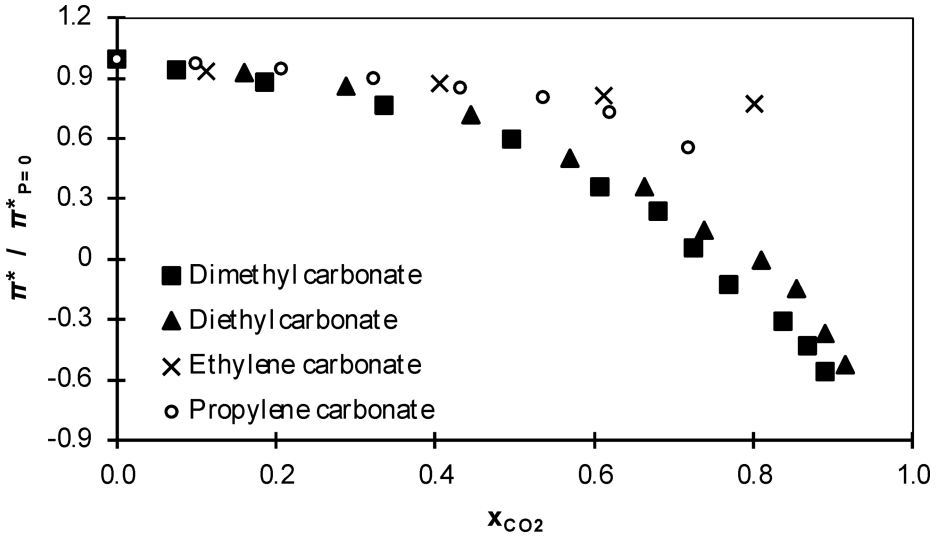

Figure 19. $\pi^*/\pi^*_{P=0}$ ratio vs x_{CO_2} for organic carbonates at the nearest available temperature of 320.2 K.

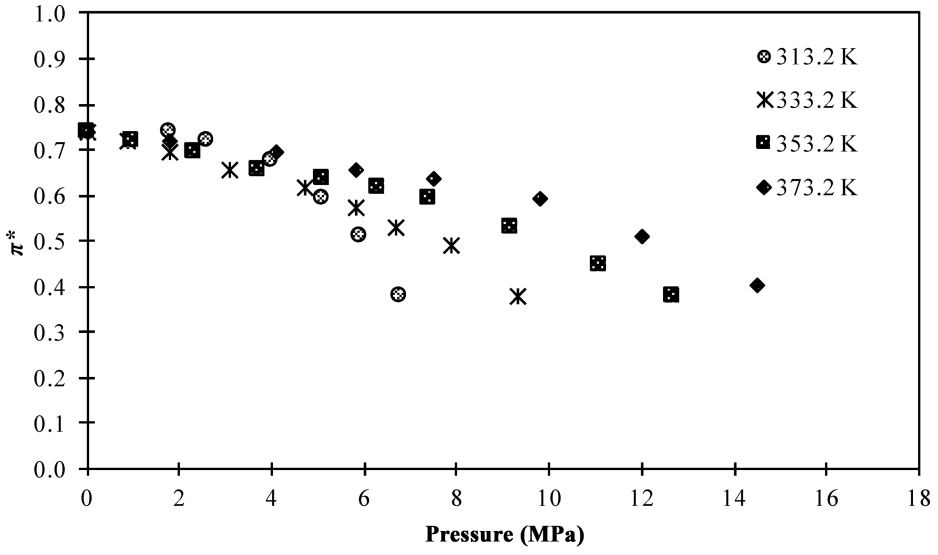

Figure 20. Variation of π^* parameter as a function of CO_2 pressure for CO_2 + anisole system at different temperatures.

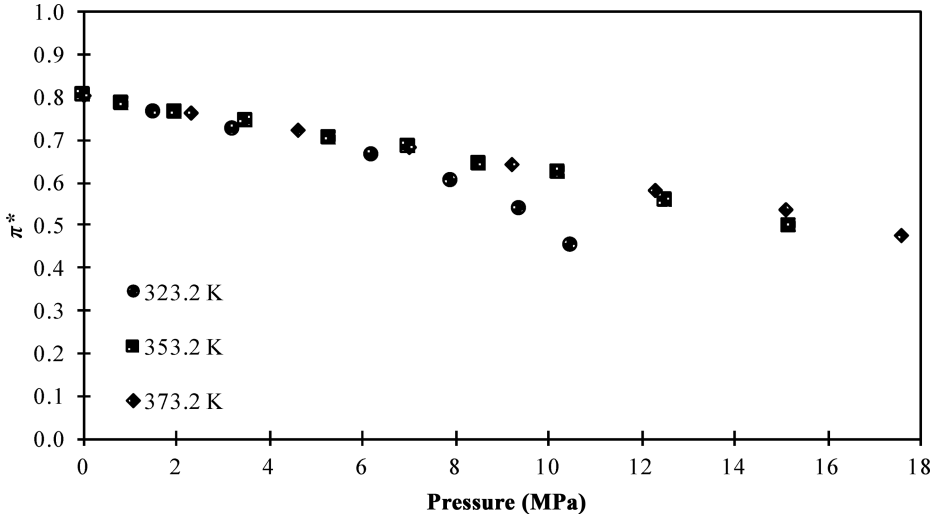

Figure 21. Variation of π^* parameter as a function of CO_2 pressure for CO_2 + veratrole system at different temperatures.

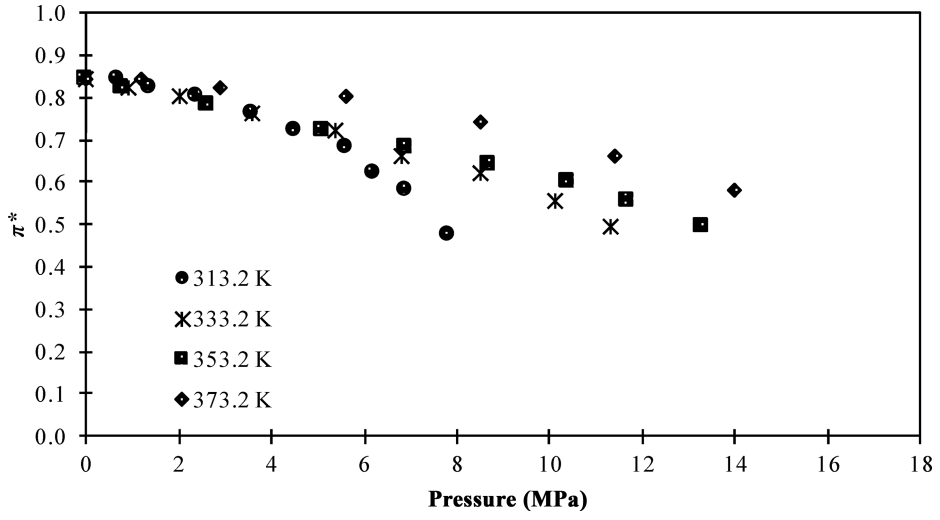

Figure 22. Variation of π^* parameter as a function of CO_2 pressure for CO_2 + γ-valerolactone system at different temperatures.

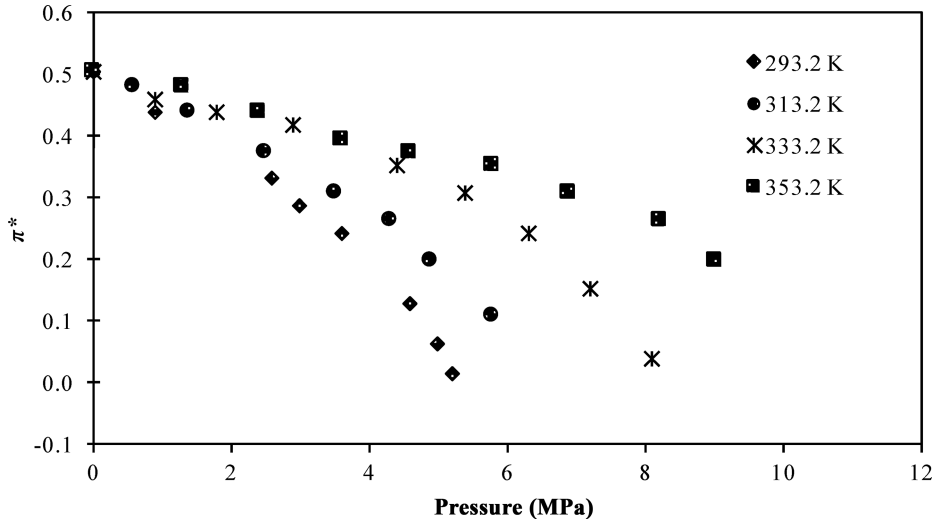

Figure 23. Variation of π^* parameter as a function of CO_2 pressure for CO_2 + 2-methyltetrahydrofuran system at different temperatures.

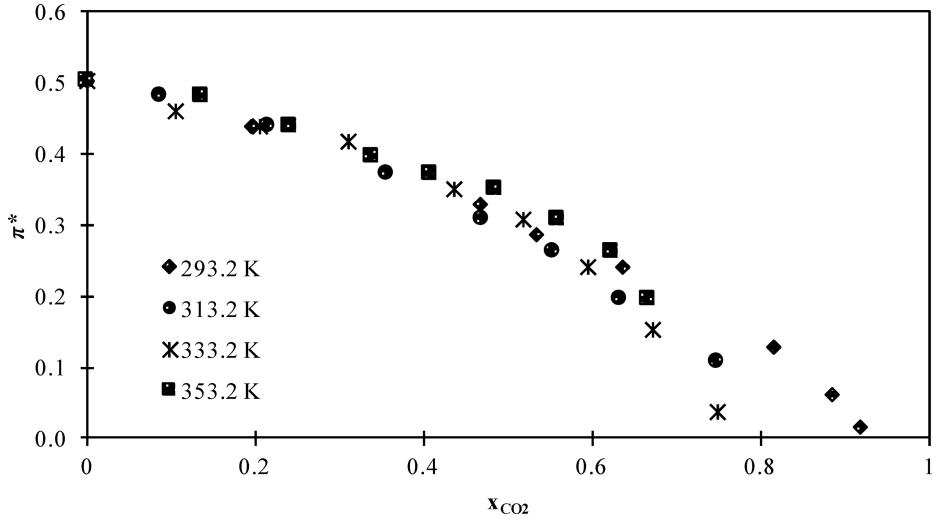

Figure 24. π^* parameter vs x_{CO_2} for CO_2-expanded 2-methyltetrahydrofuran at different temperatures.

Molecular dynamics (MD) has proved to be a very efficient methodology to estimate the density of expanded liquids. The model chosen for the CO_2 molecule (EPM2, with point charges[20] in our case) had difficulties to effectively reproduce

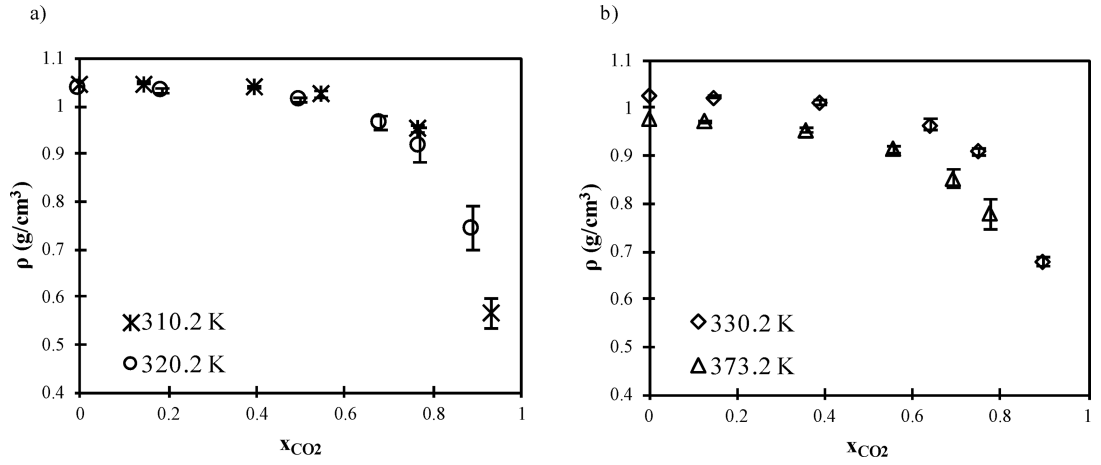

Figure 25. Density vs molar fraction for CO_2 + dimethyl carbonate system at (a) 310.2 and 320.2 K and (b) 330.2 and 373.2 K.

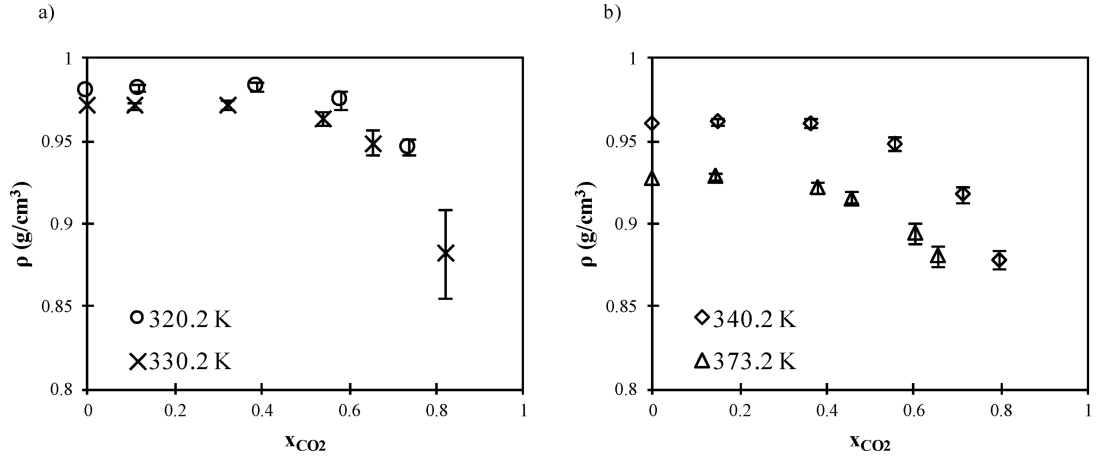

Figure 26. Density vs molar fraction for CO_2 + diethyl carbonate system at (a) 320.2 and 330.2 K and (b) 340.2 and 373.2 K.

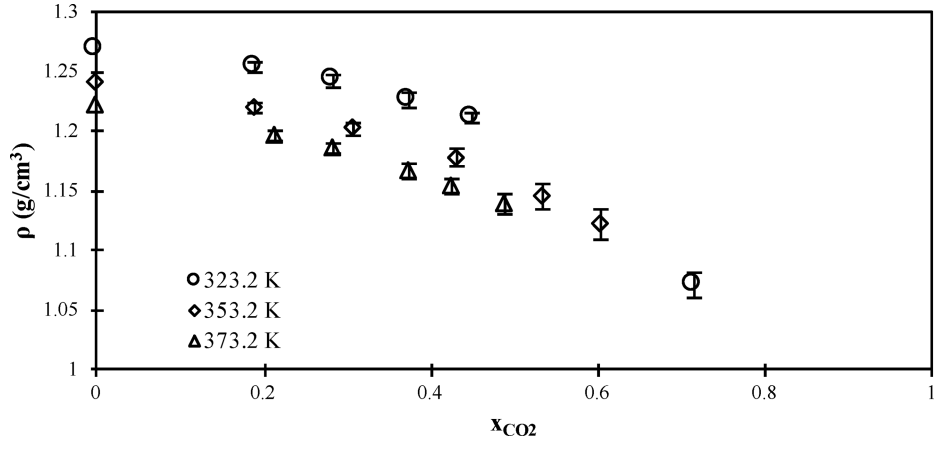

Figure 27. Density vs molar fraction for CO_2 + ethylene carbonate system at 323.2, 353.2, and 373.2 K.

the quadrupole moment of this molecule.[55a] These authors explained that the simulations with rigid models have a better performance for pure CO_2 (sub- and supercritical) whereas, for expanded systems, the model of rigid connections and flexible angle EPM2 gave the best results.

The information needed for the calculation of properties by MD, such as the composition, the pressure, and the temperature (x_{CO_2}, P, T) at equilibrium, was obtained from the literature when available or from our own determinations (section 3.1).

The following density determination results values are expressed as a function of the molar fraction of CO_2 in the expanded liquid phase (at the VLE). Density graphics contain error bars, though sometimes nearly imperceptible, and correspond to the statistical error, calculated as explained in section 2.2.2.

3.3.1. Densities of CO_2-Expanded Organic Carbonates. The evolution of the density as a function of the CO_2 mole fraction is shown in Figures 25−29. Pressures used for these calculations

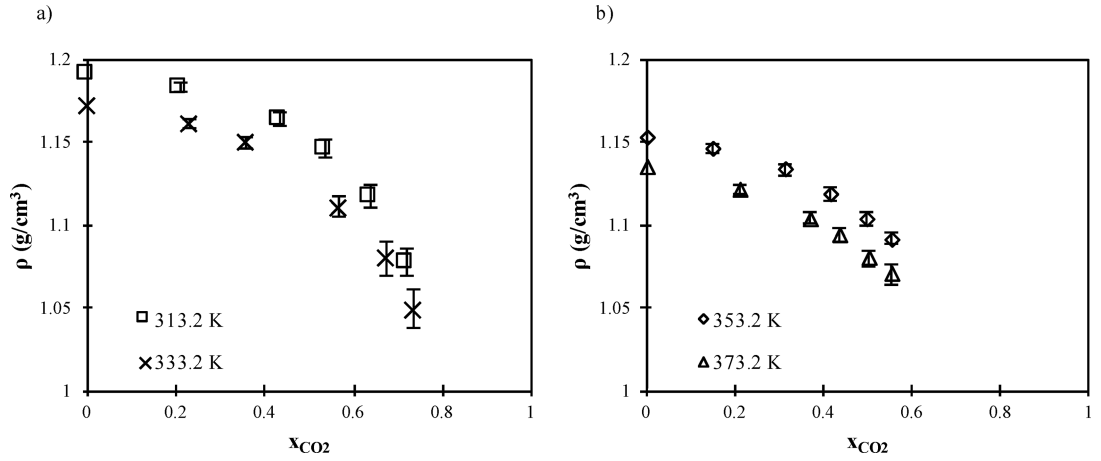

Figure 28. Density vs molar fraction for CO_2 + propylene carbonate system at (a) 313.2 and 333.2 K and (b) 353.2 and 373.2 K.

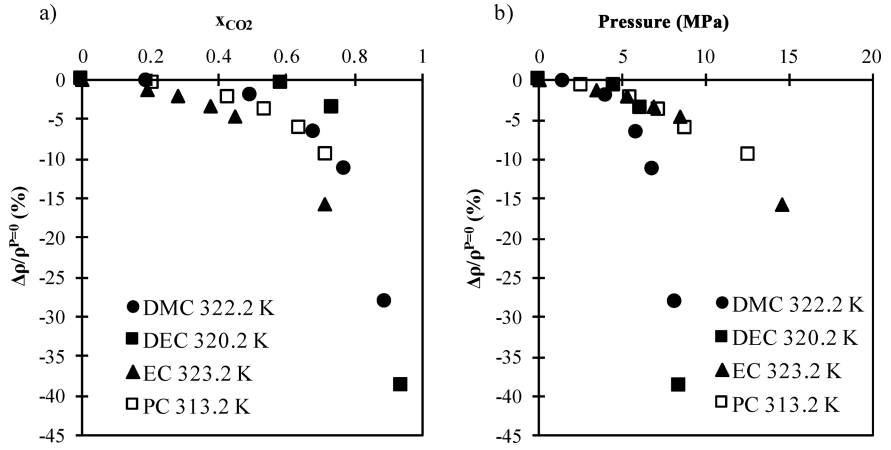

Figure 29. Change (%) in the density ratio $\Delta\rho/\rho^{P=0}$ to the pure solvent of CO_2 + organic carbonate systems as a function of mole fraction and CO_2 pressure. DMC, dimethyl carbonate; DEC, diethyl carbonate; EC, ethylene carbonate; PC, propylene carbonate.

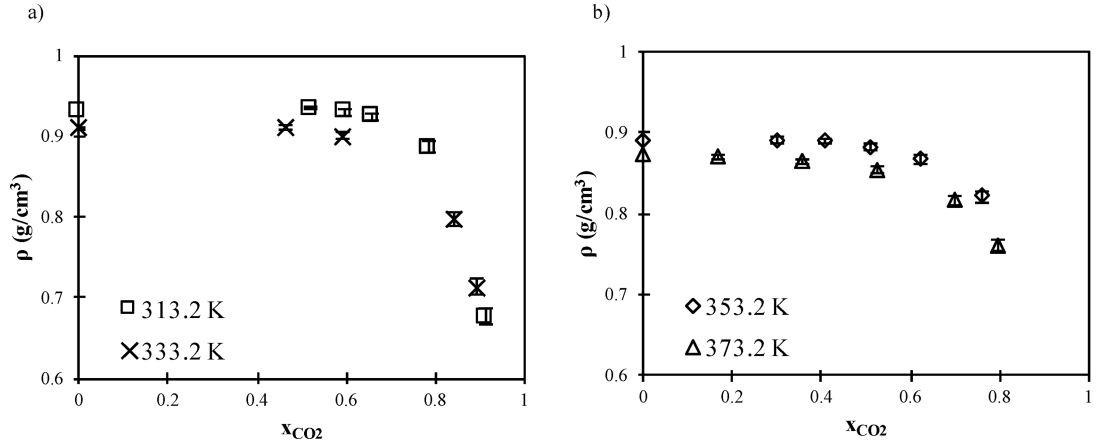

Figure 30. Density vs molar fraction for CO_2 + anisole system at (a) 313.2 and 333.2 K and (b) 353.2 and 373.2 K.

were fixed in accord with the VLE data in order to keep a biphasic system; the range of pressures used was between 1 and 30 MPa, depending on the system.

The variation of the density ratio $\Delta\rho/\rho^{P=0}$ expressed as the ratio in percent of the density variation to the density of the pure solvent can be observed in Figure 29. At first, Figure 29a shows that it is possible to modulate this ratio to values up to 45%, mainly at high CO_2 mole fractions. However, Figure 29b indicates that, to achieve these compositions in the case of cyclic carbonates (ethylene and propylene carbonates), very high pressures are required.

Concerning organic carbonates, it can then be established a trend in density modulation DMC ≈ DEC > PC ≈ EC that allows saying that modulation is higher in linear carbonates than in cyclic carbonates; this trend is confirmed by the modulation of viscosity as will be seen in section 3.4. These results come

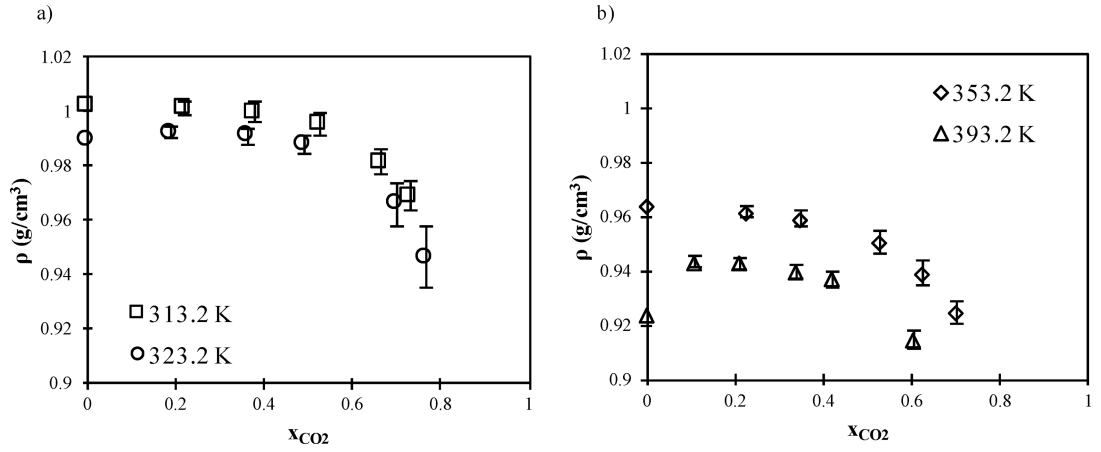

Figure 31. Density vs molar fraction for CO_2 + veratrole system at (a) 313.2 and 323.2 K and (b) 353.2 and 393.2 K.

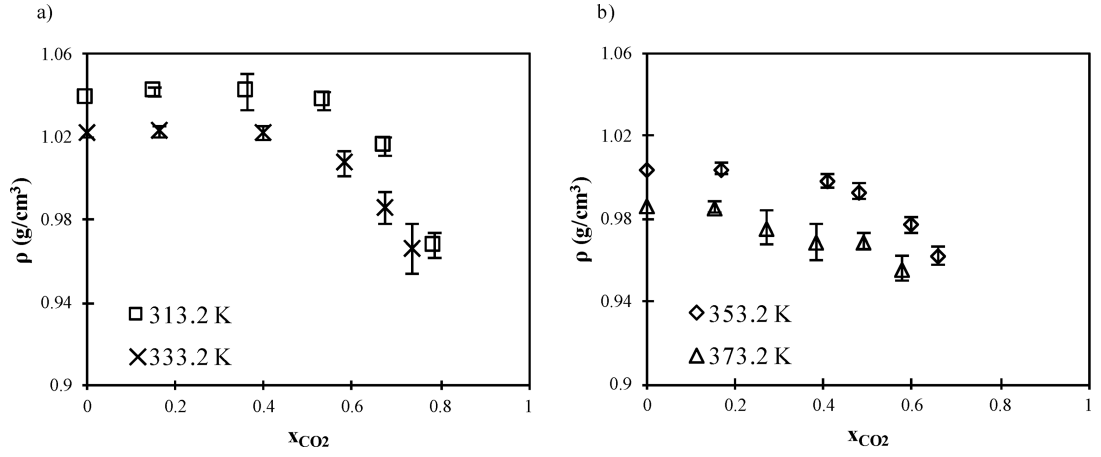

Figure 32. Density vs molar fraction for CO_2 + γ-valerolactone system at (a) 313.2 and 333.2 K and (b) 353.2 and 373.2 K.

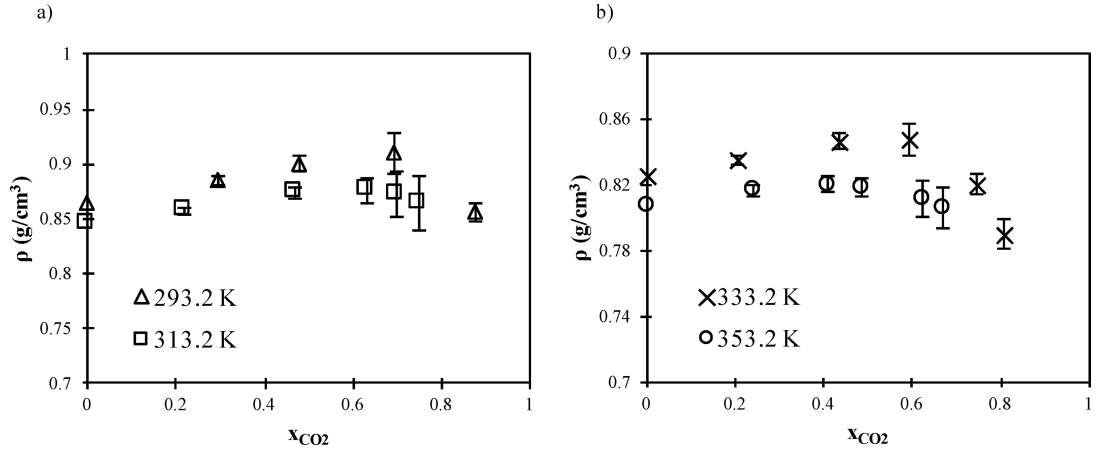

Figure 33. Density vs molar fraction for CO_2 + 2-methyltetrahydrofuran system at (a) 293.2 and 313.2 K and (b) 333.2 and 353.2 K.

from the more compact structures of cyclic carbonates compared to linear molecules, which have been evidenced by MD simulations;[55b] the compactness of these structures is accompanied by less free volume available in cyclic molecules allowing less access to CO_2 molecules and is responsible for the lower solubility of CO_2 in cyclic carbonates and for the higher density and viscosity of the neat solvent.

3.3.2. Densities of Veratrole, Anisole, γ-Valerolactone, and MeTHF Expanded by CO_2. The evolution of the density as a function of the CO_2 mole fraction is seen in Figures 30−33.

All these results indicate that the modulation of the density by the addition of CO_2 to the liquid phase is not linear with CO_2 molar fraction. Indeed, for all solvents, two zones can be distinguished. Depending on the temperature and the composition of CO_2, the density first remains almost constant or increases slightly and monotonically. Then, beyond a certain

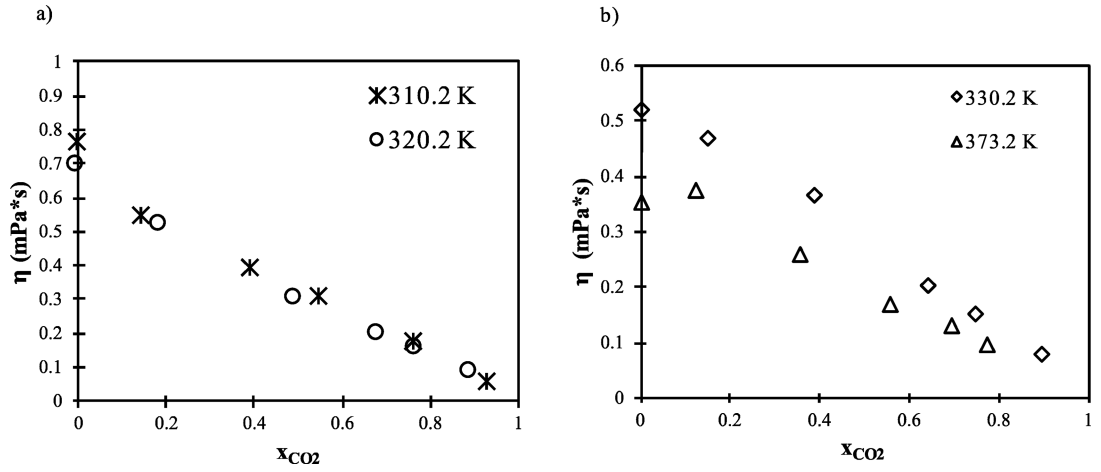

Figure 34. Viscosity vs molar fraction for CO_2 + dimethyl carbonate system at (a) 310.2 and 320.2 K and (b) 330.2 and 373.2 K.

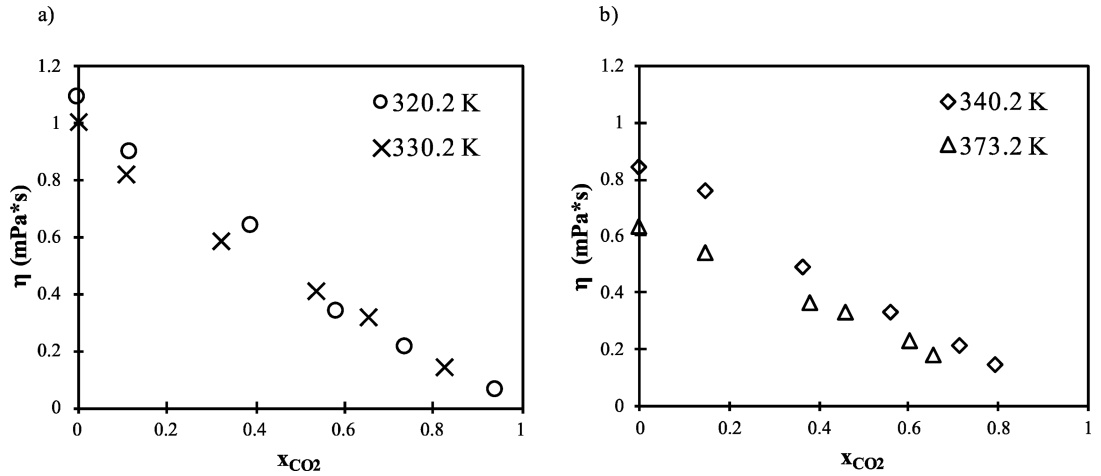

Figure 35. Viscosity vs molar fraction for CO_2 + diethyl carbonate system at (a) 320.2 and 330.2 K and (b) 340.2 and 373.2 K.

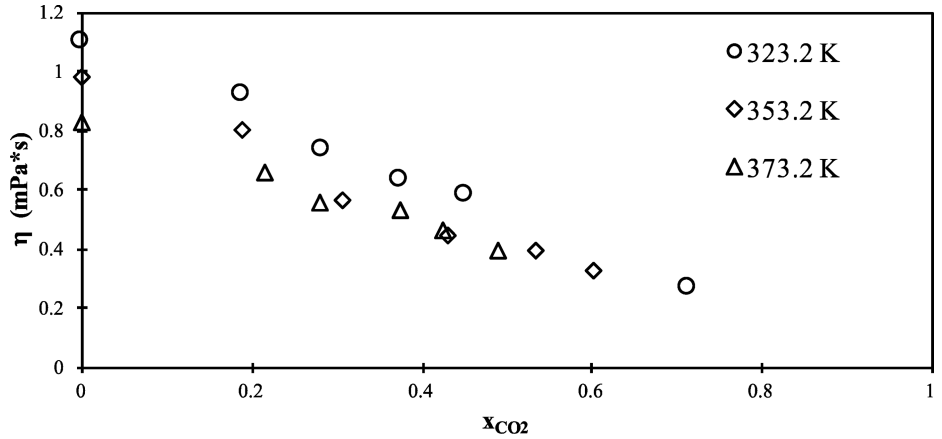

Figure 36. Viscosity vs molar fraction for CO_2 + ethylene carbonate system at 323.2, 353.2, and 373.2 K.

concentration of CO_2, a slight increment of CO_2 produces a sudden volumetric expansion and consequently a clear decrease in density. However, this concentration threshold varies considerably with temperature. This behavior is consistent with the literature[3] and was related to the increase in free volume, which would be responsible for changes in transport and solvation properties. Indeed, intermolecular voids in the pure solvent can accept CO_2 molecules to a certain extent, producing a very small increase in volume. Then, after a certain CO_2 composition threshold, its solubilization induces a rapid volume expansion. Aida et al.[56] measured the displacement of CO_2 molecules and its average orientation. This effect, capable of explaining the nonlinearity of the density with expansion, refers to the preferential localization of the CO_2 molecules around the negative charges present in the oxygens of the carbonyl groups of the carbonates, but less present in the

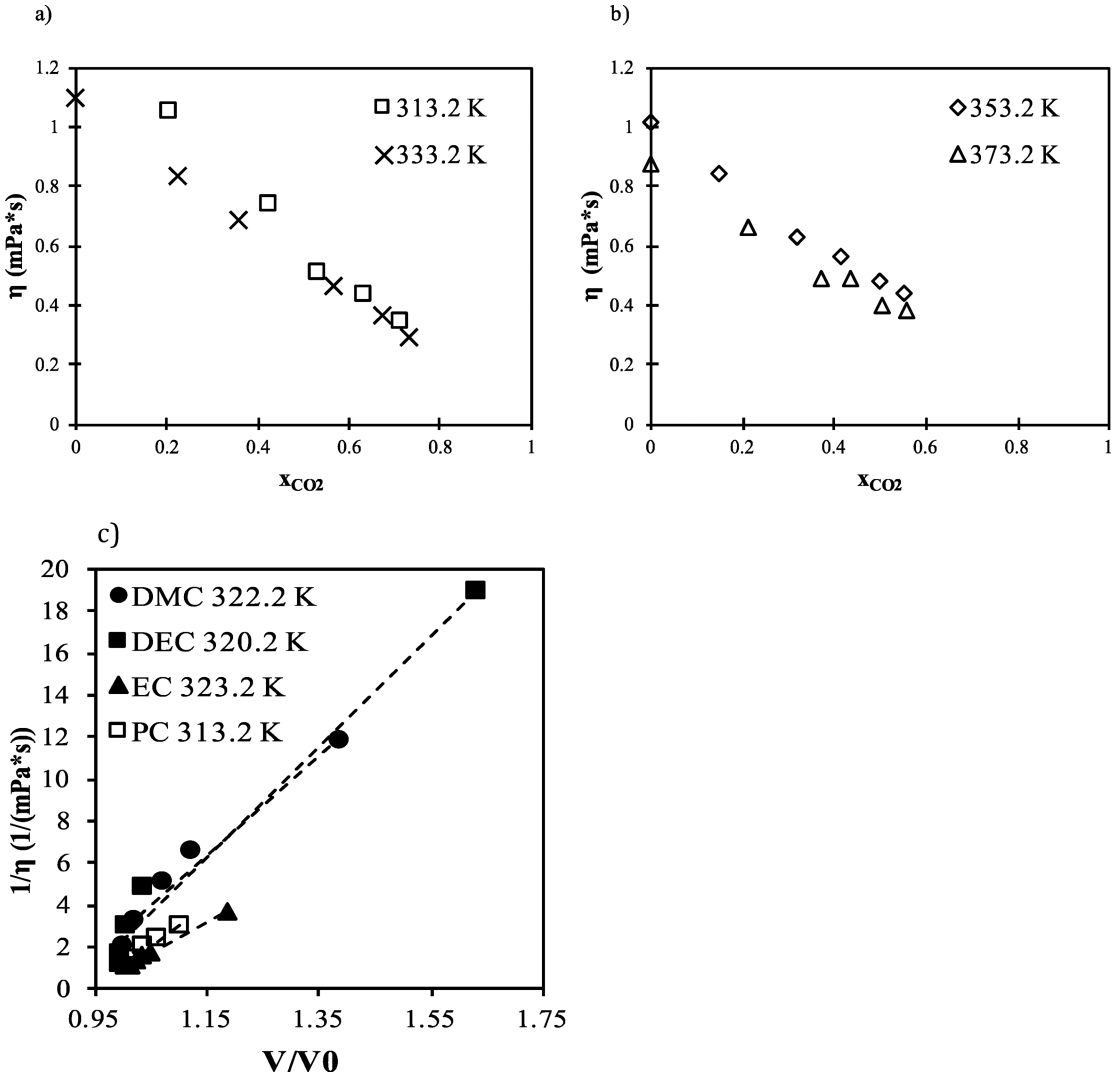

Figure 37. Viscosity vs molar fraction for CO_2 + propylene carbonate system at (a) 313.2 and 333.2 K and (b) 353.2 and 373.2 K. (c) Inverse of viscosity as a function of volume expansion for CO_2-expanded organic carbonates.

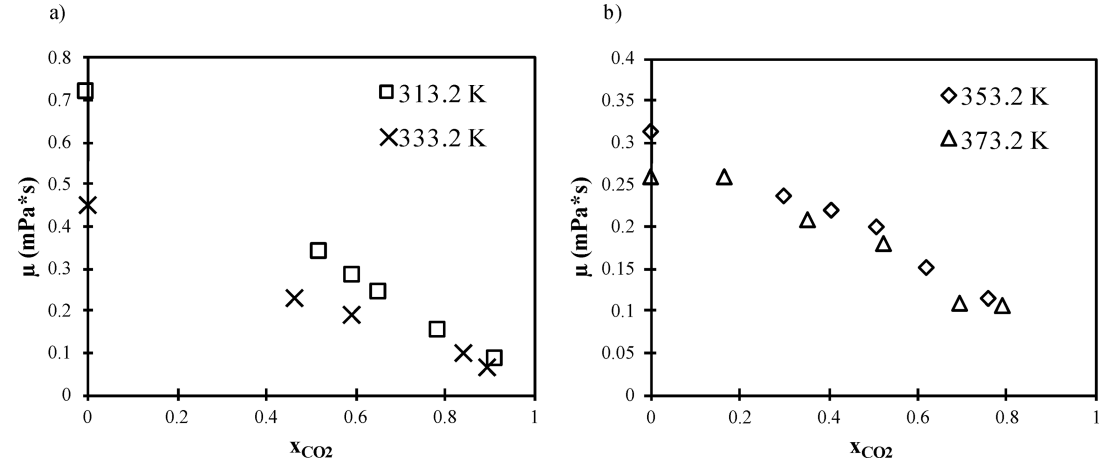

Figure 38. Viscosity vs molar fraction for CO_2 + anisole system at (a) 313.2 and 333.2 K and (b) 353.2 and 373.2 K.

oxygens of veratrole or anisole, for example, explaining therefore the visible difference between the behaviors of these solvents.

3.4. Viscosities of CO_2-Expanded Systems. The viscosities of CO_2-expanded systems have recently been investigated for other GXL systems,[4,25,57−62] showing that the presence of CO_2 in the liquid phase can significantly affect their values as well as those of other transport properties, such as diffusivities. Indeed, when CO_2 dissolves in a liquid, the viscosity

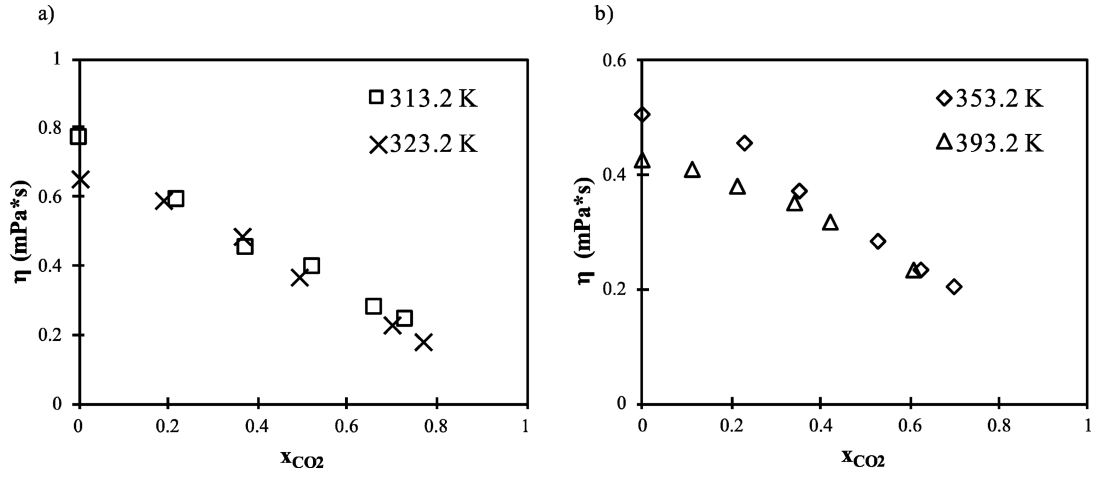

Figure 39. Viscosity vs molar fraction for CO_2 + veratrole system at (a) 313.2 and 323.2 K and (b) 353.2 and 393.2 K.

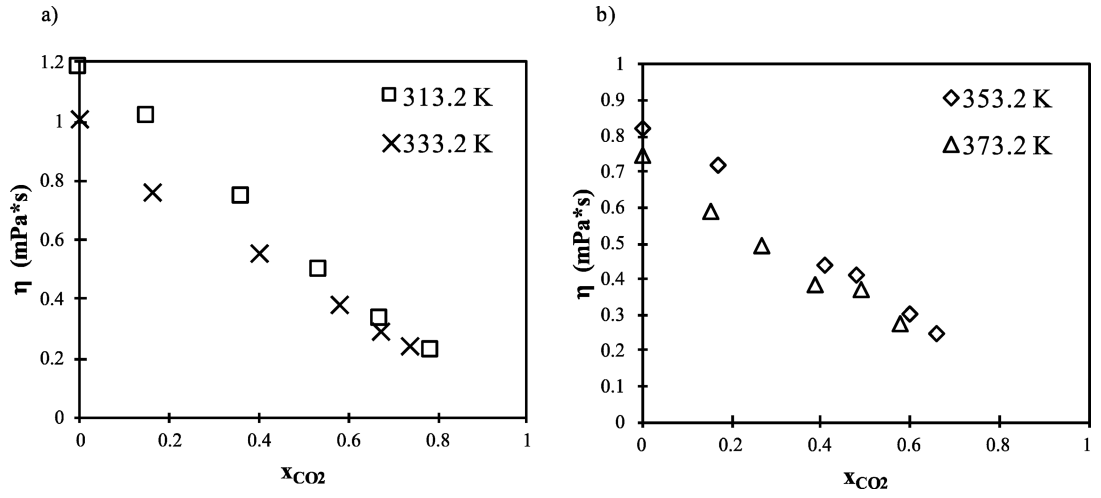

Figure 40. Viscosity vs molar fraction for CO_2 + γ-valerolactone system at (a) 313.2 and 333.2 K and (b) 353.2 and 373.2 K.

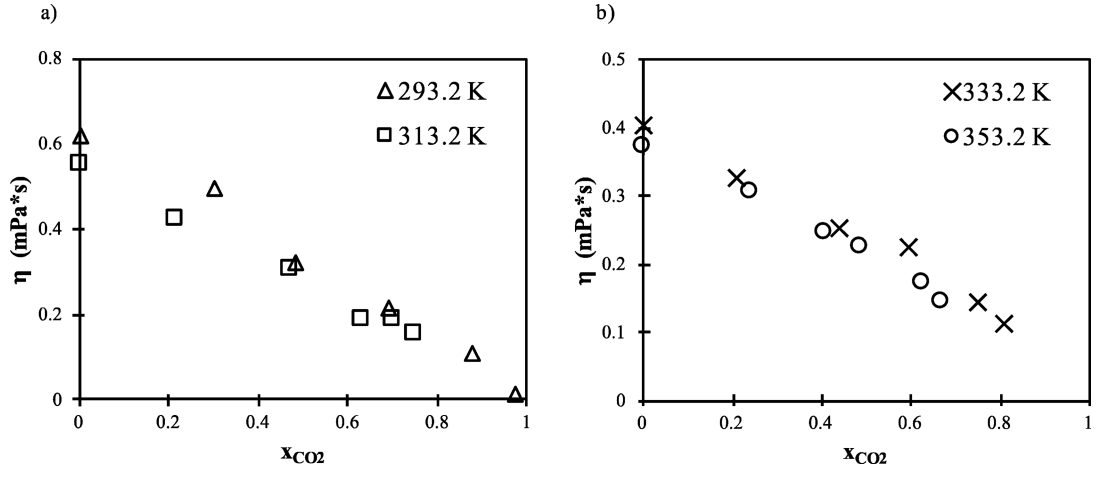

Figure 41. Viscosity vs molar fraction for CO_2 + 2-methyletetrahydrofuran system at (a) 293.2 and 313.2 K and (b) 333.2 and 353.2 K.

of this mixture can decrease significantly. From the inverse proportionality between diffusivity and viscosity as established for example by the Stokes−Einstein relation,[63] this yields an increase in diffusivity, which can greatly improve the mass transfer, an important parameter for reactor design.

For all the solvents considered here, the determination of the viscosities by molecular dynamics showed a strong decrease of this property with the addition of CO_2.

The validity of the Stokes−Einstein relationship is, however, not yet established for noncompressible systems. It has recently observed for CO_2-expanded 1-octene and CO_2-expanded

nonanal that the Stokes−Einstein relationship presents a breakdown at high concentrations of CO_2.[62b]

3.4.1. Viscosities of CO_2-Expanded Organic Carbonates. The evolution of viscosity as a function of the CO_2 concentration is seen in Figures 34−37.

To confirm the possible deviation from the Stokes−Einstein relationship for the CO_2-expanded organic carbonate systems, we have performed calculations of the inverse of viscosity (η^{-1}) vs the volume expansion, expressed as V/V_0 (Figure 37c).[62b] As can be observed, a linear dependence is observed. Further calculations for the diffusion coefficient together with experimental results would be useful to study the validity of the Stokes−Einstein relationship for these and other systems expanded by CO_2.

3.4.2. Viscosities of Anisole, Veratrole, γ-Valerolactone, and MeTHF Expanded by CO_2. The evolution of viscosity as a function of the CO_2 composition is seen in Figures 38−41.

As for pure solvents, Green−Kubo's relationship has given satisfactory results. Although the statistical error is smoothened in time, it is observed that, for some compounds, certain values seem to deviate from the global quasi-linear trend. It is considered that these singularities are attributed to error propagation in the determination of the density before launching the calculation of the viscosity in the *NVE* ensemble. Alternatively, the choice of the force field potential will impact the viscosity prediction accuracy, but this cause is ruled out here since the discrepancy occurs irregularly and only for some points.

Various factors must be separately considered to understand the modulation of the viscosity by CO_2. First, for low to moderate molar fractions, the reduction of the viscosity seems to be a quasi-linear function of the addition of CO_2 and then the reduction of the viscosity becomes less pronounced, as for example in the case of γ-valerolactone (Figure 41). It is also noted that, at constant composition, the viscosity of the expanded solvents decreases with increasing temperature, as expected.

With regard to the relation between viscosity and density, Enskog's theory[64] suggests that, if density increases, viscosity also increases. The viscosity of a fluid is closely related to the interaction of the molecules in motion. Therefore, the closer the molecules, the higher the degree of interaction. However, the densities of some organic solvents studied here may show a slight increase with the addition of CO_2 before falling sharply while the viscosity always decreases as the molar fraction of CO_2 increases. This increase in density has been attributed to the accommodation of CO_2 molecules inside the interstices between solvent molecules, leading to a transitory increase in density, up to the point where no more CO_2 molecules can be accepted and expansion arrives with a decrease in density.[4] As has recently been evidenced by Palafox-Hernandez et al. for other carbon dioxide expanded liquids (CXLs) such as 1-octene and nonanal,[62b] it is reasonable to expect that CO_2 molecules disrupt the liquid intermolecular interactions at least at high concentrations of CO_2. This disruption will undoubtedly have an impact in diffusion coefficients which would be worthwhile to determine through experimental methods together with simulations.

In conclusion, while the pressure produces very little change in pure solvents and little change for pure CO_2, in agreement with Zhong et al.,[65] the rise of CO_2 pressure in the expanded liquids studied significantly decreases the viscosity due to the dissolution of the gas. On the other hand, the temperature produces a less predictable effect, since it decreases the viscosity of the pure solvents, but at the same time decreases the dissolution of the CO_2 in the liquid. In this case, the modulation effect is thus less sensitive.

4. CONCLUSIONS

With the objective of promoting the utilization of GXLs in the industry by providing data on relevant properties for solvent engineering and simple methodologies to obtain further properties, we have studied several biomass derived solvents when expanded by CO_2. The solvents tested were dimethyl, diethyl, ethylene, and propylene carbonates, anisole, veratrole, γ-valerolactone, and 2-methyltetrahydrofuran. Experimental and molecular modeling methods were used to explore the behaviors of these fluids: phase equilibrium and the dipolarity/polarizability parameter of the expanded phase were determined experimentally while density and viscosity were determined through molecular dynamics calculations.

Comparison of our physical determinations with available literature data showed good agreement. The classification of GXLs is based precisely on the ability of the solvent to accept CO_2 and to swell; this ability to swell gives a good idea of the capacity of CO_2 to change properties such as the density, viscosity, and dipolarity of the solvent. It is clear from our results that the different solvents considered here, all derived from biomass, behave differently when in contact of CO_2: for instance, ethylene carbonate presented the lowest solubility of CO_2 among all the solvents tested while MeTHF presented the highest solubility. For a comparison, to reach a mole fraction of 0.6 at 353 K in ethylene carbonate, 30 MPa of pressure was needed, while 7.5 MPa was needed in the case of 2-methyltetrahydrofuran; mass fractions are similar in both cases and equal 0.43. From our results, it can be concluded that the solubility of CO_2 decreases when the π^* parameter of the pure compound increases; this behavior comes from the CO_2 molecule whose π^* value is very low and, depending the pressure and temperature, can be negative.

Moreover, at low concentrations, the behavior of the solvents generally showed a remarkable linearity, which would make it possible to use a simple law of the "Henry's law" type.

In relation to the π^* parameter study by solvatochromic methods, the temperature effect on the absorption spectrum of the Nile Red probe showed a hypsochromic shift (toward shorter wavelengths). The relation wavelength/temperature (thermochromism) showed a fairly linear form. These solvent-specific relations were used to "correct" π^* parameters into one reference temperature.

Analyzing the results obtained for pure solvents, in most cases the experimental π^* parameter was in very good agreement with the literature reference value (error < 0.03) except for diethyl carbonate, where the biggest difference was observed (error = 0.14).

The evolution with the pressure of the "temperature corrected" parameter π^* evidenced a great capacity of dipolarity modulation. This modulation does not, however, correspond to a linear relation between π^* and x_{CO_2}. Generally speaking, while CO_2 is introduced in the liquid phase, the π^* parameter decreases in an almost linear relation to CO_2 concentration. However, after a certain threshold, the shift in the π^* parameter becomes nonlinear and descends rapidly until pure CO_2 values; this change in tendency is higher at higher temperatures.

It follows from these determinations that it is possible to modulate the dipolarity/polarizability parameter of the GXL in a range from the dipolarity of the pure solvent to that of pure CO_2 and allows replacing a given conventional solvent by a binary mixture with similar solvation properties that possibly can be adjusted when needed. For instance, if we observe the case of 2-methyltetrahydrofuran, the dipolarity modulation range goes from $\pi^* = 0.53$ to negative π^* values which corresponds to pure CO_2 (depending on temperature). Other interesting cases that show the great capacities for modulation of the π^* parameter by CO_2 are by anisole, veratrole, and γ-valerolactone where π^* values of the pure solvent can be divided by 2 when CO_2 is added at pressures as low as 5 MPa.

As far as the expansion phenomenon is concerned, we have seen that it is possible to modulate the density largely by adding CO_2, from pure solvent densities in the range 850−1100 kg/m^3 to the density of pure CO_2. For instance, diethyl carbonate reached nearly half its density when the CO_2 concentration was about 0.9. Depending on the solvent, the density may increase slightly at the beginning or remain relatively constant as long as the liquid accepts the molecules of the gas in the intermolecular interstices. Once this capacity is exceeded, the density decreases when the concentration of gas increases.

The gas solubilization in the liquid phase produces a decrease in viscosity as expected. However, this effect was observed as quasi-linear and it occurs even at low concentrations of CO_2, where the density shows a slight increase. This is probably one of the biggest advantages of GXLs, because modulation occurs in all the range of compositions, and in a soft tendency depending on molar fraction. Temperature had a notorious effect on GXL viscosity both because of the increase in mobility of the pure solvent and because of the decreased CO_2 solubility. In opposition to pure fluids where mechanical pressure has little or no effect on viscosity, CO_2 pressure and thus its concentration allow a great viscosity modulation. All solvents studied here showed a similar behavior when comparing viscosity behaviors as a function of CO_2 molar fraction. More viscous solvents such as propylene carbonate (μ = 1.4 at 313.2 K) and less viscous solvents such as 2-methyltetrahydrofuran (μ = 0.6 at 293.2 K) behaved evenly and their viscosities decreased to nearly half at $x_{CO_2} = 0.5$. Viscosity seems to affect the CO_2 absorption rate, with the viscous solvents taking more time to dissolve CO_2 and to arrive at a stable pressure. It is, however, worth noting that the validity of the Stokes−Einstein relationship is still to demonstrate by calculation and experimental determinations of the diffusivity in these systems. Disruption of the liquid intermolecular interaction by CO_2 is still demonstrated through the determination of diffusivity in these systems.

Concerning organic carbonates, a trend was observed, where the solubility of CO_2 and, consequently, the possibility of modulation of properties is higher in linear carbonates than in cyclic carbonates, which is consistent with previous studies concerning compactness of similar molecules.

GXLs have been studied over the past two decades; nevertheless, they are still in the first steps of development. The application on an industrial scale of GXLs is currently very limited as are the data available in the literature. Most of the work on this topic has focused on the study of the liquid phase expansion phenomenon, but very few studies have presented a quantitative evaluation of all other properties of these systems while they are needed to promote their use as a smart alternative to conventional solvents. This work essentially aims at providing some data to fill this gap.

AUTHOR INFORMATION

Corresponding Author

*E-mail: yaocihuatl.medinagonzalez@ensiacet.fr or yaocihuatl.medinagonzalez-ext@solvay.com.

ORCID

Yaocihuatl Medina-Gonzalez: 0000-0003-2859-8158

Present Address

§Centre National de Recherche Scientifique, University of Bordeaux, Solvay, LOF, UMR 5258 CNRS Solvay, 33600 Pessac, France.

Notes

The authors declare no competing financial interest.

ACKNOWLEDGMENTS

The authors deeply thank CALMIP (Calcul en Midi-Pyrénées (UMS CNRS 3667)) for the hours allocated in the supercomputer facility (Project No. P1535).

REFERENCES

(1) Jessop, P. G.; Subramaniam, B. Gas-Expanded Liquids. *Chem. Rev.* **2007**, *107* (6), 2666−2694.

(2) *Gas-Expanded Liquids and Near-Critical Media: Green Chemistry and Engineering*; Hutchenson, K. W., Scurto, A. M., Subramaniam, B., Eds.; ACS Symposium Series 1006; American Chemical Society: 2009.

(3) Abbott, A. P.; Hope, E. G.; Mistry, R.; Stuart, A. M. Probing the Structure of Gas Expanded Liquids Using Relative Permittivity, Density and Polarity Measurements. *Green Chem.* **2009**, *11* (10), 1530−1535.

(4) Li, H.; Maroncelli, M. Solvation and Solvatochromism in CO_2-Expanded Liquids. 1. Simulations of the Solvent Systems CO_2 + Cyclohexane, Acetonitrile, and Methanol. *J. Phys. Chem. B* **2006**, *110* (42), 21189−21197.

(5) Akien, G. R.; Poliakoff, M. A Critical Look at Reactions in Class I and II Gas-Expanded Liquids Using CO_2 and Other Gases. *Green Chem.* **2009**, *11* (8), 1083.

(6) Medina-Gonzalez, Y.; Jarray, A.; Camy, S.; Condoret, J. S.; Gerbaud, V. CO_2-Expanded Alkyl Lactates: A Physicochemical and Molecular Modeling Study. *J. Solution Chem.* **2017**, *46* (2), 259−280.

(7) Aida, T.; Aizawa, T.; Kanakubo, M.; Nanjo, H. Analysis of Volume Expansion Mechanism of CO_2-Acetate Systems at 40 °C. *J. Supercrit. Fluids* **2010**, *55* (1), 56−61.

(8) Granero-Fernandez, E.; Machin, D.; Lacaze-Dufaure, C.; Camy, S.; Condoret, J.-S.; Gerbaud, V.; Charpentier, P. A.; Medina-Gonzalez, Y. CO_2-Expanded Alkyl Acetates: Physicochemical and Molecular Modeling Study and Applications in Chemical Processes. *ACS Sustainable Chem. Eng.* **2018**, *6* (6), 7627−7637.

(9) Hoang, H. N.; Granero-Fernandez, E.; Yamada, S.; Mori, S.; Kagechika, H.; Medina-Gonzalez, Y.; Matsuda, T. Modulating Biocatalytic Activity toward Sterically Bulky Substrates in CO_2-Expanded Biobased Liquids by Tuning the Physicochemical Properties. *ACS Sustainable Chem. Eng.* **2017**, *5* (11), 11051−11059.

(10) Brunner, G. *Gas Extraction*; Topics in Physical Chemistry 4; Steinkopff: Heidelberg, 1994. DOI: 10.1007/978-3-662-07380-3.

(11) Crampon, C.; Charbit, G.; Neau, E. High-Pressure Apparatus for Phase Equilibria Studies: Solubility of Fatty Acid Esters in Supercritical CO_2. *J. Supercrit. Fluids* **1999**, *16* (1), 11−20.

(12) Kamlet, M. J.; Taft, R. W. The Solvatochromic Comparison Method. I. The β-Scale Of Solvent Hydrogen-Bond Acceptor (HBA) Basicities. *J. Am. Chem. Soc.* **1976**, *98* (2), 377−383.

(13) Taft, R. W.; Kamlet, M. J. The Solvatochromic Comparison Method. 2. The α-Scale of Solvent Hydrogen-Bond Donor (HBD) Acidities. *J. Am. Chem. Soc.* **1976**, *98* (10), 2886−2894.

(14) Kamlet, M. J.; Abboud, J. L.; Taft, R. W. The Solvatochromic Comparison Method. 6. The Π* Scale of Solvent Polarities. *J. Am. Chem. Soc.* **1977**, *99* (18), 6027−6038.
(15) Taft, R. W.; Abboud, J. L. M.; Kamlet, M. J.; Abraham, M. H. Linear Solvation Energy Relations. *J. Solution Chem.* **1985**, *14* (3), 153−186.
(16) *Materials and Process Simulation (MAPS)*; Scienomics: 2017.
(17) (a) Martyna, G. J.; Tobias, D. J.; Klein, M. J. Constant pressure molecular dynamics algorithms. *J. Chem. Phys.* **1994**, *101*, 4177. (b) Frisch, M. J.; Trucks, G. W.; Schlegel, H. B.; Scuseria, G. E.; Robb, M. A.; Cheeseman, J. R.; Scalmani, G.; Barone, V.; Mennucci, B.; Petersson, G. A.; et al. *Gaussian 09*; Gaussian, Inc.: 2016.
(18) Singh, U. C.; Kollman, P. A. An Approach to Computing Electrostatic Charges for Molecules. *J. Comput. Chem.* **1984**, *5* (2), 129−145.
(19) Besler, B. H.; Merz, K. M.; Kollman, P. A. Atomic Charges Derived from Semiempirical Methods. *J. Comput. Chem.* **1990**, *11* (4), 431−439.
(20) Harris, J. G.; Yung, K. H. Carbon Dioxide's Liquid-Vapor Coexistence Curve And Critical Properties as Predicted by a Simple Molecular Model. *J. Phys. Chem.* **1995**, *99* (31), 12021−12024.
(21) Frenkel, D.; Smit, B. Molecular Dynamics Simulation. In *Understanding Molecular Simulation: From Algorithms to Application*; Academic Press: 2002; pp 63−107. DOI: 10.1016/B978-012267351-1/50006-7.
(22) Kubo, R. The Fluctuation-Dissipation Theorem. *Rep. Prog. Phys.* **1966**, *29* (1), 255.
(23) Green, M. S. Markoff Random Processes and the Statistical Mechanics of Time-Dependent Phenomena. II. Irreversible Processes in Fluids. *J. Chem. Phys.* **1954**, *22* (3), 398−413.
(24) Kubo, R. Statistical-Mechanical Theory of Irreversible Processes. I. General Theory and Simple Applications to Magnetic and Conduction Problems. *J. Phys. Soc. Jpn.* **1957**, *12* (6), 570−586.
(25) Houndonougbo, Y.; Laird, B. B.; Kuczera, K. Transport Properties of CO_2-Expanded Acetonitrile from Molecular Dynamics Simulations. *J. Chem. Phys.* **2007**, *126* (7), 074507.
(26) Cui, S. T.; Cummings, P. T.; Cochran, H. D. The Calculation of Viscosity of Liquid N-Decane and n-Hexadecane by the Green−Kubo Method. *Mol. Phys.* **1998**, *93* (1), 117−122.
(27) Nevins, D.; Spera, F. J. Accurate Computation of Shear Viscosity from Equilibrium Molecular Dynamics Simulations. *Mol. Simul.* **2007**, *33* (15), 1261−1266.
(28) Dysthe, D. K.; Fuchs, A. H.; Rousseau, B. Prediction of Fluid Mixture Transport Properties by Molecular Dynamics. *Int. J. Thermophys.* **1998**, *19*, 437−448.
(29) Guevara-Carrion, G.; Nieto-Draghi, C.; Vrabec, J.; Hasse, H. Prediction of Transport Properties by Molecular Simulation: Methanol and Ethanol and Their Mixture. *J. Phys. Chem. B* **2008**, *112* (51), 16664−16674.
(30) Im, J.; Kim, M.; Lee, J.; Kim, H. Vapor-Liquid Equilibria of Binary Carbon Dioxide + Alkyl Carbonate Mixture Systems. *J. Chem. Eng. Data* **2004**, *49* (2), 243−245.
(31) Camy, S.; Pic, J. S.; Badens, E.; Condoret, J. S. Fluid Phase Equilibria of the Reacting Mixture in the Dimethyl Carbonate Synthesis from Supercritical CO_2. *J. Supercrit. Fluids* **2003**, *25* (1), 19−32.
(32) Hongling, L.; Rongjiao, Z.; Wei, X.; Yanfen, L.; Yongju, S.; Yiling, T. Vapor-Liquid Equilibrium Data of the Carbon Dioxide + Ethyl Butyrate and Carbon Dioxide + Propylene Carbonate Systems at Pressures from (1.00 to 13.00) MPa and Temperatures from (313.0 to 373.0) K. *J. Chem. Eng. Data* **2011**, *56* (4), 1148−1157.
(33) Williams, L. L.; Mas, E. M.; Rubin, J. B. Vapor - Liquid Equilibrium in the Carbon Dioxide - Propylene Carbonate System at High Pressures. *J. Chem. Eng. Data* **2002**, *47*, 282−285.
(34) Walther, D.; Maurer, G. High-Pressure Vapor-Liquid Equilibria for CO_2 + Benzonitrile, CO_2 + Benzyl Alcohol, CO_2 + 2-Tert-Butylphenol, CO_2 + Methoxybenzene, and CO_2 + 1,2,3,4-Tetrahydronaphthalene at Temperatures between 313. *J. Chem. Eng. Data* **1993**, *38* (2), 247−249.
(35) Park, S. Do; Kim, C. H.; Choi, C. S. High-Pressure Binary Vapor-Liquid Equilibrium Measurements of Carbon Dioxide with Aromatic Hydrocarbons. *J. Chem. Eng. Data* **1991**, *36* (1), 80−84.
(36) Kim, C. H.; Clark, A. B.; Vimalchand, P.; Donohue, M. D. High-Pressure Binary Phase Equilibria of Aromatic Hydrocarbons with Carbon Dioxide and Ethane. *J. Chem. Eng. Data* **1989**, *34* (4), 391−395.
(37) Lee, M. J.; Kou, C. F.; Cheng, J. W.; Lin, H. mu. Vapor-Liquid Equilibria for Binary Mixtures of Carbon Dioxide with 1,2-Dimethoxybenzene, 2-Methoxyphenol, or p-Cresol at Elevated Pressures. *Fluid Phase Equilib.* **1999**, *162* (1−2), 211−224.
(38) Shiflett, M. B.; Yokozeki, A. Solubility of CO_2 in Room Temperature Ionic Liquid [Hmim][Tf_2N]. *J. Phys. Chem. B* **2007**, *111* (8), 2070−2074.
(39) Ren, W.; Sensenich, B.; Scurto, A. M. High-Pressure Phase Equilibria of {carbon Dioxide (CO_2) + n-Alkyl-Imidazolium Bis-(Trifluoromethylsulfonyl)Amide} Ionic Liquids. *J. Chem. Thermodyn.* **2010**, *42* (3), 305−311.
(40) Deng, D.; Han, G.; Jiang, Y.; Ai, N. Solubilities of Carbon Dioxide in Five Biobased Solvents. *J. Chem. Eng. Data* **2015**, *60* (1), 104−111.
(41) Mistry, R. *Characterisation and Applications of CO_2-Expanded Solvents*; University of Leicester: 2008.
(42) Golini, C. M.; Williams, B. W.; Foresman, J. B. Further Solvatochromic, Thermochromic, and Theoretical Studies on Nile Red. *J. Fluoresc.* **1998**, *8* (4), 395−404.
(43) Kawski, A.; Kukliński, B.; Bojarski, P. Photophysical Properties and Thermochromic Shifts of Electronic Spectra of Nile Red in Selected Solvents. Excited States Dipole Moments. *Chem. Phys.* **2009**, *359* (1−3), 58−64.
(44) Ito, M. The Effect of Temperature on Ultraviolet Absorption Spectra and Its Relation to Hydrogen Bonding. *J. Mol. Spectrosc.* **1960**, *4* (1−6), 106−124.
(45) Kamlet, M. J.; Abboud, J. L. M.; Abraham, M. H.; Taft, R. W. Linear Solvation Energy Relationships. 23. A Comprehensive Collection of the Solvatochromic Parameters, π, α, and β, and Some Methods for Simplifying the Generalized Solvatochromic Equation. *J. Org. Chem.* **1983**, *48* (17), 2877−2887.
(46) Jessop, P. G.; Jessop, D.; Fu, D.; Phan, L. Solvatochromic Parameters for Solvents of Interest in Green Chemistry. *Green Chem.* **2012**, *14*, 1245.
(47) Wyatt, V. T.; Bush, D.; Lu, J.; Hallett, J. P.; Liotta, C. L.; Eckert, C. A. Determination of Solvatochromic Solvent Parameters for the Characterization of Gas-Expanded Liquids. *J. Supercrit. Fluids* **2005**, *36* (1), 16−22.
(48) Królicki, R.; Jarzęba, W.; Mostafavi, M.; Lampre, I. Preferential Solvation of Coumarin 153 - The Role of Hydrogen Bonding. *J. Phys. Chem. A* **2002**, *106* (9), 1708−1713.
(49) Hallett, J. P.; Kitchens, C. L.; Hernandez, R.; Liotta, C. L.; Eckert, C. A. Probing the Cybotactic Region in Gas-Expanded Liquids (GXLs). *Acc. Chem. Res.* **2006**, *39* (8), 531−538.
(50) Gutkowski, K. I.; Fernández-Prini, R.; Aramendía, P. F.; Japas, M. L. Critical Effects on Attractive Solutes in Binary Liquid Mixtures Close to Their Consolute Point: A New Experimental Strategy. *J. Phys. Chem. B* **2011**, *115* (51), 15303−15312.
(51) Tanaka, Y.; Kawashima, Y.; Yoshida, N.; Nakano, H. Solvatochromism and Preferential Solvation of Brooker's Merocyanine in Water-methanol Mixtures. *J. Comput. Chem.* **2017**, *38* (28), 2411−2419.
(52) Sayadian, M.; Khaleghian, M.; Yari, M. Solvatochromism and Preferential Solvation in Mixtures of Methanol with Ethanol, 1-Propanol and 1-Butanol. *Orient. J. Chem.* **2014**, *30* (4), 1897−1903.
(53) Li, H.; Arzhantsev, S.; Maroncelli, M. Solvation and Solvatochromism in CO_2-Expanded Liquids. 2. Experiment-Simulation Comparisons of Preferential Solvation in Three Prototypical Mixtures. *J. Phys. Chem. B* **2007**, *111* (12), 3208−3221.
(54) Swalina, C.; Arzhantzev, S.; Li, H.; Maroncelli, M. Solvatochromism and Solvation Dynamics in CO_2-Expanded Liquids. *In ACS Symposium Series* **2009**, *1006*, 95−111.
(55) (a) Aimoli, C. G.; Maginn, E. J.; Abreu, C. R. A. Force Field Comparison and Thermodynamic Property Calculation of Supercritical

CO_2 and CH_4 Using Molecular Dynamics Simulations. *Fluid Phase Equilib.* **2014**, *368*, 80−90. (b) Alatas, P. V.; Tsalikis, D. G.; Mavrantzas, V. G. Detailed molecular dynamics simulation of the structure and self-diffusion of linear and cyclic n-alkanes in melt and blends. *Macromol. Theory Simul.* **2017**, *26* (1), 1600049.

(56) Aida, T.; Aizawa, T.; Kanakubo, M.; Nanjo, H. Dependence of Volume Expansion on Alkyl Chain Length and the Existence of Branched Methyl Group of CO_2-Expanded Ketone Systems at 40 °C. *J. Supercrit. Fluids* **2010**, *55* (1), 71−76.

(57) Cullick, A. S.; Mathis, M. L. Densities and Viscosities of Mixtures of Carbon Dioxide and N-Decane from 310 to 403 K and 7 to 30 MPa. *J. Chem. Eng. Data* **1984**, *29* (4), 393−396.

(58) Sih, R.; Foster, N. R. Viscosity Measurements on Saturated Gas Expanded Liquid Systems-Acetone and Carbon Dioxide. *J. Supercrit. Fluids* **2008**, *47* (2), 233−239.

(59) Sih, R.; Armenti, M.; Mammucari, R.; Dehghani, F.; Foster, N. R. Viscosity Measurements on Saturated Gas-Expanded Liquid Systems—Ethanol and Carbon Dioxide. *J. Supercrit. Fluids* **2008**, *43* (3), 460−468.

(60) Matsuda, H.; Kurihara, K.; Tochigi, K.; Funazukuri, T.; Rattan, V. K. Estimation of Kinematic Viscosities for CO_2-Expanded Liquids by ASOG-VISCO Model. *Fluid Phase Equilib.* **2018**, *470*, 188−192.

(61) Sih, R.; Dehghani, F.; Foster, N. R. Viscosity Measurements on Gas Expanded Liquid Systems—Methanol and Carbon Dioxide. *J. Supercrit. Fluids* **2007**, *41* (1), 148−157.

(62) (a) Houndonougbo, Y.; Kuczera, K.; Subramaniam, B.; Laird, B. B. Prediction of Phase Equilibria and Transport Properties in Carbon-Dioxide Expanded Solvents by Molecular Simulation. *Mol. Simul.* **2007**, *33*, 861−869. (b) Palafox-Hernandez, J. P.; Mendis, C. H.; Thompson, W. H.; Laird, B. B. Pressure and temperature tuning of gas-expanded liquid structure and dynamics. *J. Phys. Chem. B* **2019**, *123*, 2915−2924.

(63) Einstein, A. Über Die von Der Molekularkinetischen Theorie Der Wärme Geforderte Bewegung von in Ruhenden Flüssigkeiten Suspendierten Teilchen. *Ann. Phys.* **1905**, *322* (8), 549−560.

(64) Poling, B. E.; Prausnitz, J. M.; O'Connell, J. P. *The Properties of Gases and Liquids*; McGraw-Hill: New York, 2001; Vol. 5.

(65) Zhong, H.; Lai, S.; Wang, J.; Qiu, W.; Lüdemann, H.-D.; Chen, L. Molecular Dynamics Simulation of Transport and Structural Properties of CO_2 Using Different Molecular Models. *J. Chem. Eng. Data* **2015**, *60* (8), 2188−2196.